CODING AND ITERATIVE DEMODUATION FOR OFDM ON DOUBLY-SELECTIVE COMMUNICATIONS CHANNELS

by

Zahraalsadat Alavizadeh

Submitted in partial fulfillment of the requirements
for the degree of Master of Applied Science

at

Dalhousie University
Halifax, Nova Scotia
August 2017

To my parents, Masih and Fatemeh, who always supported me, whatever path I took. Thanks for your endless love and advices.

Table of Contents

List of Figures

Abstract

The purpose of this research is to design an OFDM system to apply for an underwater acoustic environment. In this study we face several challenges such as decreasing multipath and Doppler effect and increasing the capacity of the system. We use an LDPC and repetition coded sytem to equalize the channel without using high-complexity equalization algorithms. By designing an iterative cancellation loop, we iteratively cancel interference and Doppler effect in time-varying channels. In addition, in order to increase the capacity and to improve the system performance, we added more hydrophones to the receiver. Finally, in order to increase the transmission rate, we expand our model to multiple-input multiple-output system by adding more users to transmit their data.

List of Abbreviations Used

AWGN	Additive White Gaussian Nosie
BER	Bit Error Rate
CP	Cyclic Prefix
DQPSK	Differential Quadrature Phase Shift Keying
FFT	Fast Fourier Transform
ICI	InterChannel Interference
iFFT	inverse Fast Fourier Transform
ISI	InterSymbol Interference
LLR	Log-Likelihood Ratio
MF	Matched Filter
MIMO	Multiple-Input Multiple-Output
OFDM	Orthogonal Frequency Division Multiplexing
QPSK	Quadrature Phase Shift Keying
RA	Repeat-Accumulate
RX	Receiver
SIMO	Single-Input Multiple-Output
SISO	Single-Input Single-Output
TX	Transmitter

Acknowledgements

Firstly, I would like to express my sincere gratitude to my advisor Prof.Schlegel for the support of my master study and related research, for his patience, motivation, and knowledge. His guidance helped me in all the time of this research. I would like to thank you very much for your support and understanding over these past two years.

I am extremly thankful to Dr.Trukhachev, Lukas Grinewitschus, post-doc fellows and Navid Eskandari who greatly assisted the research.

I would also like to show gratitude to my family who offered their encouragement through this research.

Chapter 1

Introduction

In this thesis, we introduced an OFDM system using LDPC and repetition code, an iterative cancelation loop and applied this system to a semi-analytical channel modeling of an underwater acoustic environment. The purpose of designing such a system is to cancel the Doppler spread effect, detect the signal in the presence of multipath effect without using complex equalization methods and increase the capacity. The reflections of acoustic signals from the sea surface and bottom and the refraction of signals by the spatially varying sound speed in the water column results in multiple propagation paths. Moreover, the biggest contribution of the random Doppler effects on the channel are due to surface gravity waves, and, combined with motion-induced Doppler shifts, present the dominant source of Doppler effects.

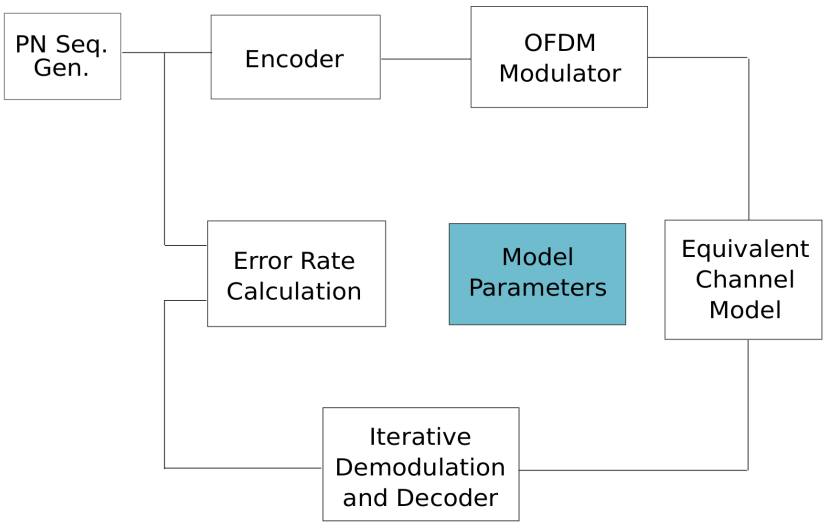

Figure 1.1: Block diagram of the SISO system.

Progress in this area concentrates on the following highlights: We designed a single-input multiple-output transceiver, 1. In this system we added OFDM modulation as a multicarrier modulation method. A large number of subcarriers carry data on parallel data streams. The advantage of OFDM is to address several problems

such as fading due to multipath while in conventional communication systems these issues were very challenging. Moreover, by a single matrix multiplication we can equalize a frequency-selective channel. We have also added an LDPC coded system as coding system, especially the high-rate IEEE 802.3an (32,6) code. Experiments with this code have, however, revealed that this particular code may not be ideally suited to the highly dynamic acoustic channel since it is very sensitive to outages of symbols. We designed other LDPC codes that also are tested for suitability. Moreover, a low-rate, high-diversity repetition coded system can equalize the channel very successfully, and examples are shown in this thesis. Both systems assume that the transmission channel is *known exactly*. An iterative cancelation loop was implemented for both systems, which allows to iteratively cancel interference without resorting to high-complexity equalization algorithms. In addition, in conventional wireless communications, a single transducer is used at the transmitter and a single hydrophone at the receiver.

In the rest of this thesis, a combination of multiple hydrophones is considered and their benefits are quantified. We consider single-input multiple-output (SIMO) systems, with a single transmit transducer and multiple receive hydrophones. Moreover, SIMO helps to improve the system performance by increasing channel capacity and spectrum efficiency. Finally, we expand the SIMO system into a MIMO and explain its performance.

Chapter 2

Orthogonal Frequency-Division Multiplexing (OFDM) and Channel Model

Orthogonal Frequency Division Multiplexing (OFDM) is a multi carrier modulation and it can be considered as a multiplexing method. In OFDM we divide the signal bandwidth into parallel subcarriers. Dividing channel into smaller subchannels makes OFDM signal more robust against frequency selective fading. In OFDM transmission, the transmitted signal is generated from data signals of size N symbols that are defined in the frequency domain, and then transformed via a discrete fourier transform into a sequence of time-domain samples. These are typically augmented by a cyclic prefix of size $M \ll N$. For details see [1]. if $N \gg M$ as in the usual case, the rate loss due to the insertion of the cyclic prefix is minimal. On the other hand, the cyclic prefix has the advantage of converting complex intersymbol interference channels into much more managable diagonal vector channels as outlined below.

The output samples in the time domain, denoted by $\boldsymbol{y}$, after adding and removing the CP, can be written in time-domain vector form as [5]

$$\boldsymbol{y} = \mathbf{H}\boldsymbol{x} + \boldsymbol{\psi} \tag{2.1}$$

where

$$\mathbf{H} = \begin{bmatrix} f_1 & & & & f_L & \cdots & f_2 \\ \vdots & f_1 & & & & \ddots & \vdots \\ \vdots & \vdots & \ddots & & & & f_L \\ f_L & \vdots & \ddots & f_1 & & & \\ & f_L & \ddots & \vdots & f_1 & & \\ & & \ddots & \vdots & \vdots & \ddots & \\ & & & f_L & f_{L-1} & \cdots & f_1 \end{bmatrix} \tag{2.2}$$

and $\mathbf{x}$ is the vector of N time-domain samples that result from the DFT operation

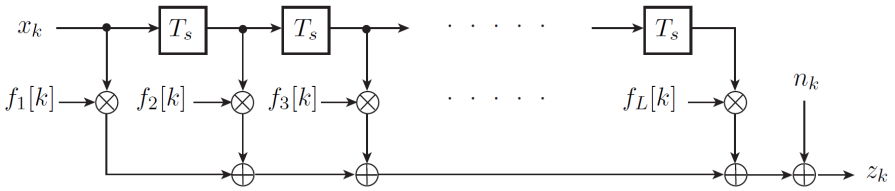

Figure 2.1: Tapped delay-line model of the same multipath fading channel.

on the original frequency-domain symbols $\mathbf{X}$. The vector $\boldsymbol{\psi}$ is additive channel noise. The coefficients f_i are complex values that represent tap values the discrete FIR filter, Figure 2, that describes the transmission of the time-domain samples $\boldsymbol{x}$ through the channel. Due to the addition of the cyclic prefix, $\mathbf{H}$ is an $N \times N$ circulant matrix. The discrete fourier transform diagonalizes all circulant matrices and we obtain the frequency-domain expression after the DFT given by

$$\begin{aligned} \mathbf{Y} &= \mathbf{F^H} \boldsymbol{y} \\ &= \mathbf{F^H H F} \left(\boldsymbol{y} + \boldsymbol{\psi} \right) \\ &= \mathbf{H}^{(f)} \boldsymbol{X} + \boldsymbol{\Psi} \end{aligned} \tag{2.3}$$

where

$$\mathbf{H}^{(f)} = \mathbf{F^H H F} = \begin{bmatrix} H[0] & & \\ & \ddots & \\ & & H[N-1] \end{bmatrix} \tag{2.4}$$

is a *diagonal* frequency gain matrix [5]. However, in the case of rapidly time-selective channels, typical of acoustic underwater channels, the fourier transform in (2.4) produces off-diagonal elements since the rows of the time-domain matrix (2.2) are no longer exact shift of each other as the equivalent filter tap coefficients f_i become time-, and therefore row-dependent. These off-diagonal elements are, in fact, inter-channel interference (ICI), in the sense that signal X_i causes responses in Y_j where $j = i \pm i'$, and i' are the indices of the neighboring frequences that are "contaminated" by the signal X_i.

As a general rule-of-thumb we know that the delay spread in the channel translates into the fluctuations of the diagonal and upper/lower diagonals of $\mathbf{H}^{(f)}$, while the

rapidity of the time-variations of the coefficients f_i, or more precisely their doppler spectrum, translates into the width of the band-diagonal of $\mathbf{H}^{(f)}$. This OFDM system is tested with a "five-path" test channel model with impulse responses at the discrete time $n = 0$ carrying 30% of the energy followed by other impulses carrying 30% of the energy at $n = 3$, 20% at $n = 6$, 10% at $n = 9$ and 10% at $n = 12$. This standard delay power profile is shown in Figure 2.2.

Additionally, each path is modeled as a fading process with a Doppler power spectrum created by a stretched exponential function. The channels we simulate use the stretched exponential model with a stretching exponent $\beta = 1$, i.e., the two-sided exponential function is used, with the Doppler power spectrum

$$S_C(\nu) = \frac{1}{2\alpha}\, e^{-|\nu|/\alpha} \tag{2.5}$$

where ν is the Doppler frequency and α is the root-mean-square doppler spread. Analogous to the mean relaxation time in time-domain exponential models, α can be called the "mean relaxation frequency" of the Doppler power spectrum. A higher mean relaxation frequency means higher Doppler frequencies are present in the channel, causing a wider Doppler power spectrum.

This channel model is a semi-analytical model, and as such assumes that we have acquired frame synchronization. We will also assume that the channel is known exactly.

The channel model does capture the time variability of the channel, which expresses itself in off-diagonal terms that appear in the frequency-domain channel matrix $\mathbf{H}^{(f)}$. These off-diagonal terms constitute inter-channel interference (ICI). Figure 2.3 shows the magnitudes of $\mathbf{H}^{(f)}$ for a relative rms Doppler spread number of $a = \alpha N T_s = 1$. This would imply that the coherence time of the channel $T_{\text{coh}} \leq 1/(NT_s)$, hence the ICI components. This channel presents a significant problem for conventional signaling methods.

We present an iterative equalization system that can communicate effectively over this channel, as well as channels with much larger rms Doppler numbers $a > 1$.

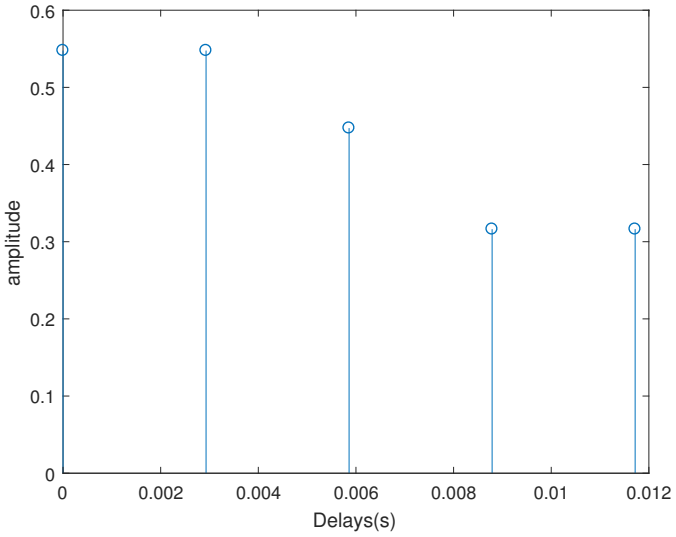

Figure 2.2: Standard channel delay profile for our test channel, generated by the matlab setup code AcousticDynamicChannel.m.

Figure 2.4 shows some examples of the time variations impressed by various doppler models on the $N = 1024$ samples of a single OFMD frame.

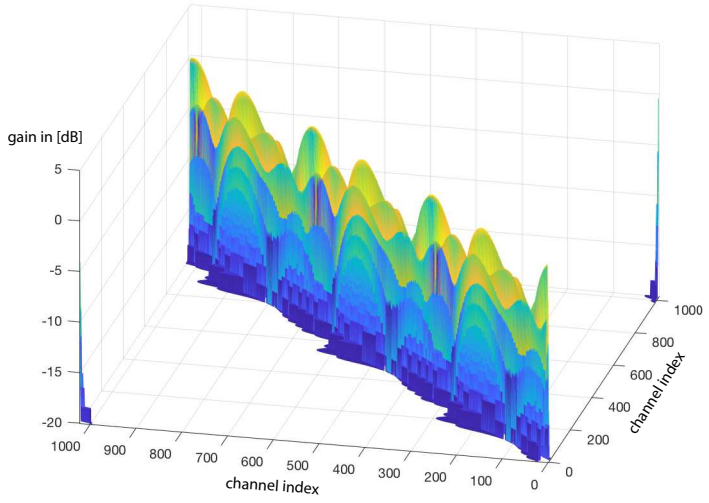

Figure 2.3: Frequency gains of doubly dispersive fading channel as used in this thesis.

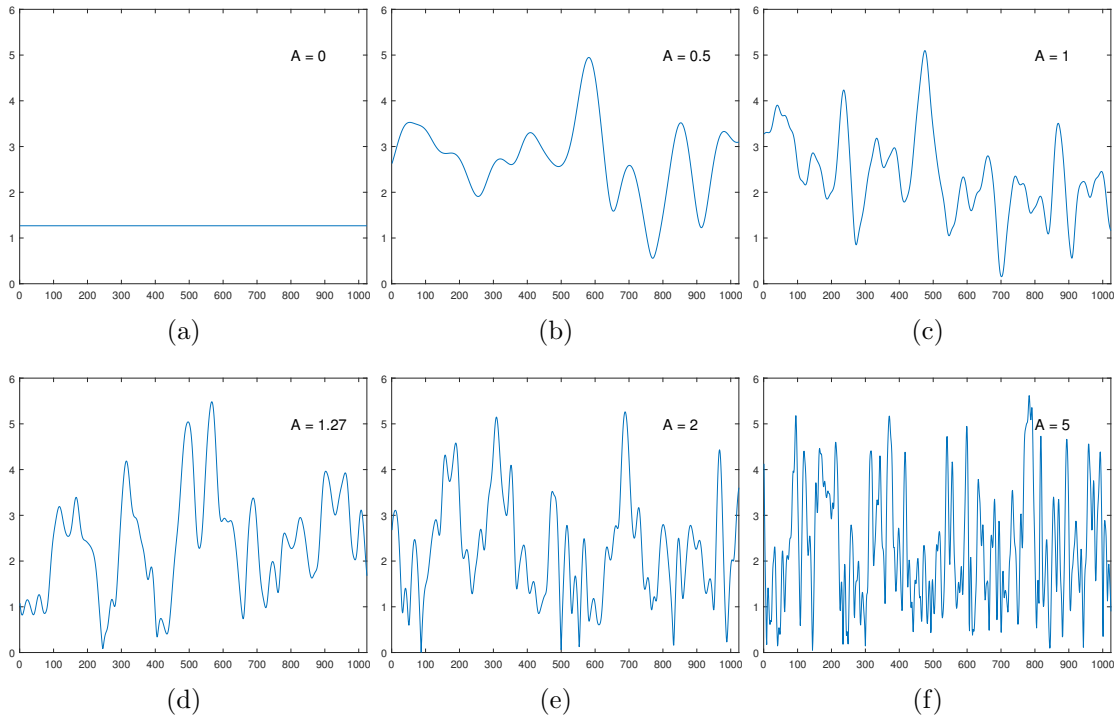

Figure 2.4: Examples of time variation throughout a single OFDM frame for different A.

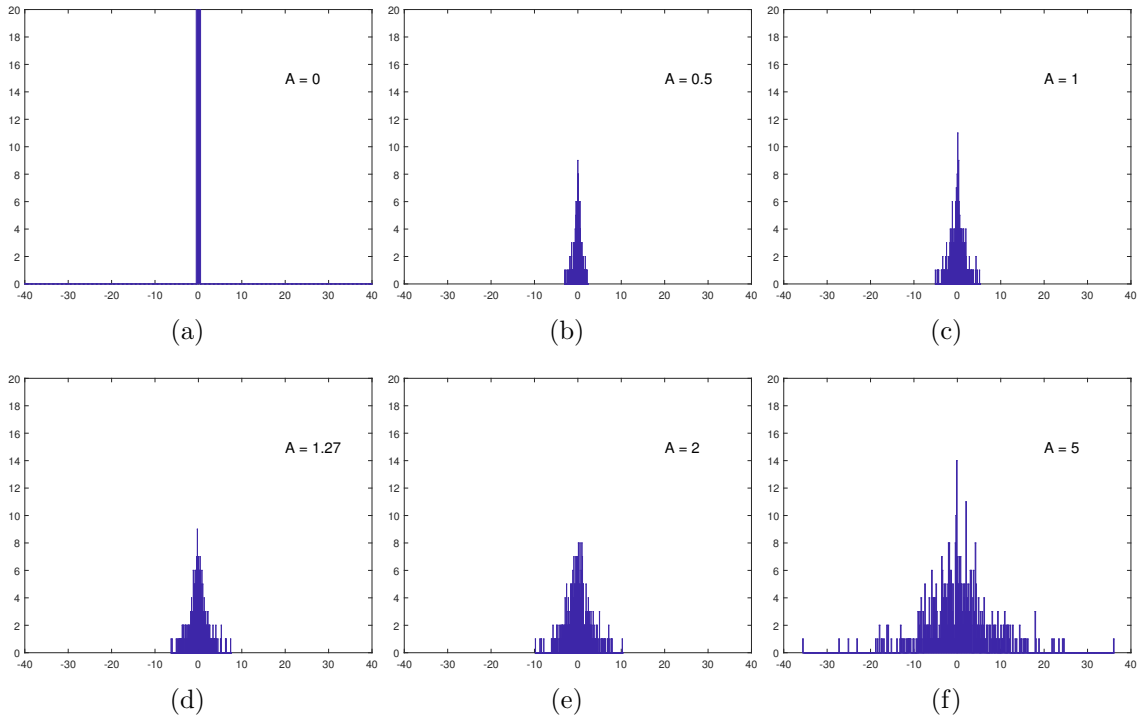

Figure 2.5: Histogram of doppler frequencies for different A's.

2.1 Channel Model of a Real Environment

In the previous section, we defined a simple channel delay profile to test our system. In order to test our algorithm in a more realistic environment, we use two channel models: the first one is a channel with correlated fading among the paths and the second model has uncorrelated fading. When we transmit a signal, the propagating acoustic wave reaches the surface and bottom of sea, where it is reflected back into the body of water, as illustrated in Figure 4.1. If the locations of the sea surface that are hit by different propagating waves are in close proximity—on the order of the length of a typical surface water wave—, the reflected signals will be highly correlated.

We produce these channel models using the Bellhop modeling software, which is used to generate the channel matrix for the power delay profile of each hydrophone. The sound speed profile data for shallow water for the Atlantic Ocean and for St.Margarets bay are used to produce the gains and delays of each path. Figure 2.6 shows the power delay profile of five channels for a 5-element receive array. The maximum delay in the echo arrivals is 80 T_s where T_s is the sampling time, that is, the inverse of the sampling frequency $f_s = 320$ Hz. The channel macro parameters are

$$\tau_{\max} = 80\ T_s; \qquad f_s = 1/T_s = 320\ \text{Hz}\,. \tag{2.6}$$

We define $\mathbf{H}$ as the aggregate frequency-domain channel matrix, and the H_ks are the individual channel matrices. Furthermore, $\mathbf{R_k} = \mathbf{H_k}^H\mathbf{H_k}$ is frequency-domain correlation matrix for the k-th hydrophone. Figure 2.8 shows the matrix $\mathbf{R}$ for a single and the aggregate of the five-element array for the uncorrelated fading scenario. Due to the smoother diagonal variation in matrix R of the system with 5 hydrophones, it has a better performance than the system with correlated fading over all paths, shown in Figure 2.7 which depicts the $\mathbf{R}$ matrices for correlated fading case.

While $\tau_{\max}$ defines the frequency-selectivity of the channel, its time-selectivity is determined by the doppler spread of the different path. Doppler effects are caused by motion of the TX or RX, or that of the medium itself, such as the wave action. We give this motion a time-dependent velocity $v(t)$, which implies a time-dependent *Mach number* $a(t) = 1 + v(t)/c$, where c is the speed of sound in water.

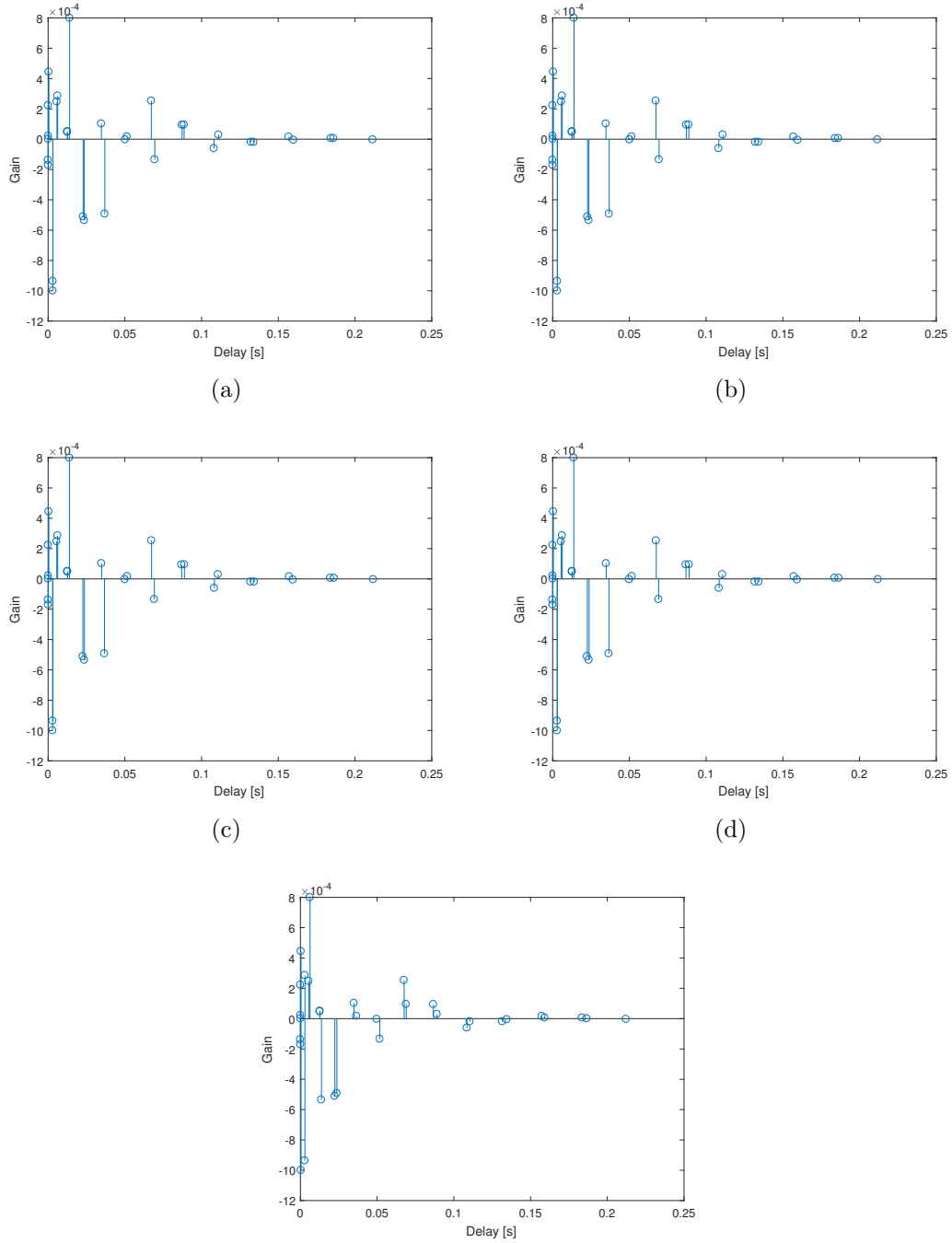

Figure 2.6: Channel delay profiles for a SIMO channel where the receive hydrophones are located between 30 m to 31.5 m in shallow water. The maximum delay spread is $\tau_{max} = 80\,T_s$ at a sampling frequency of $f_s = 320$ Hz.

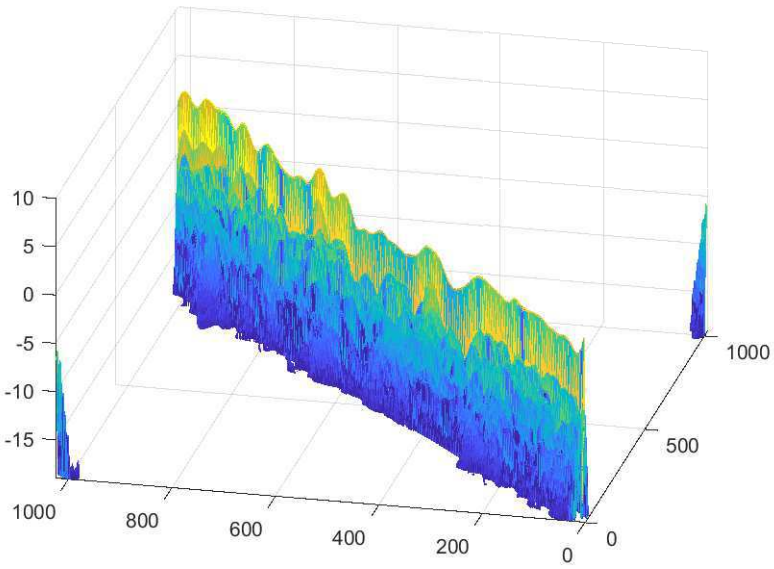

(a)

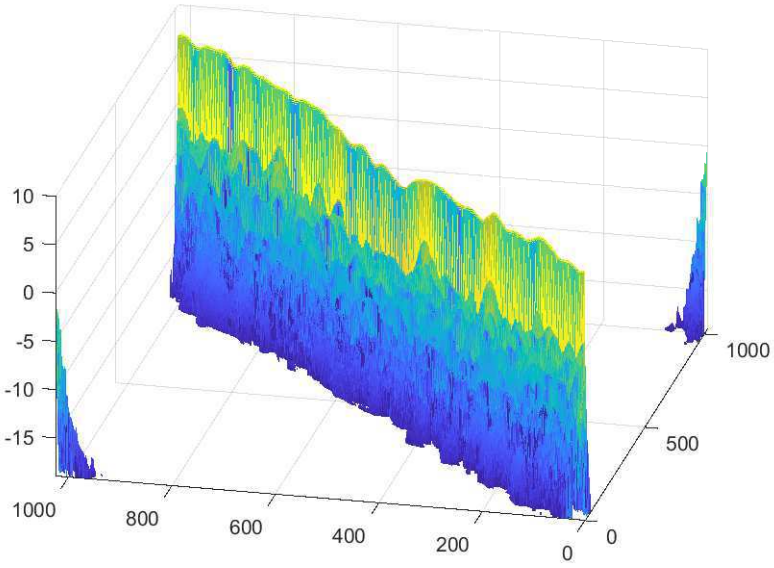

(b)

Figure 2.7: **R**-matrix for uncorrelated fading., Figure 2.7(a): matrix **R** for one hydrophone. Figure 2.7(b): matrix **R** for the entire SIMO system for $A = 1$, which would be a heavy sea state. The transmitter is at 30 m and five hydrophones are between 30 m and 31.5 m depth.

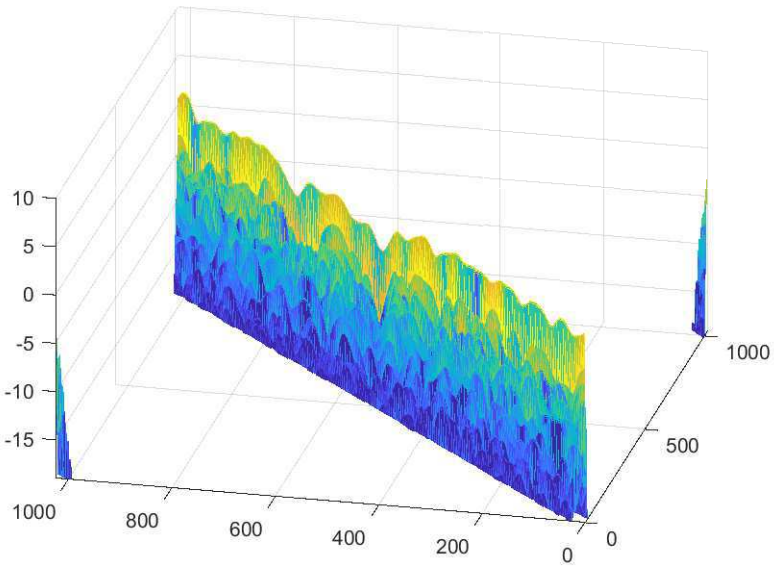

(a)

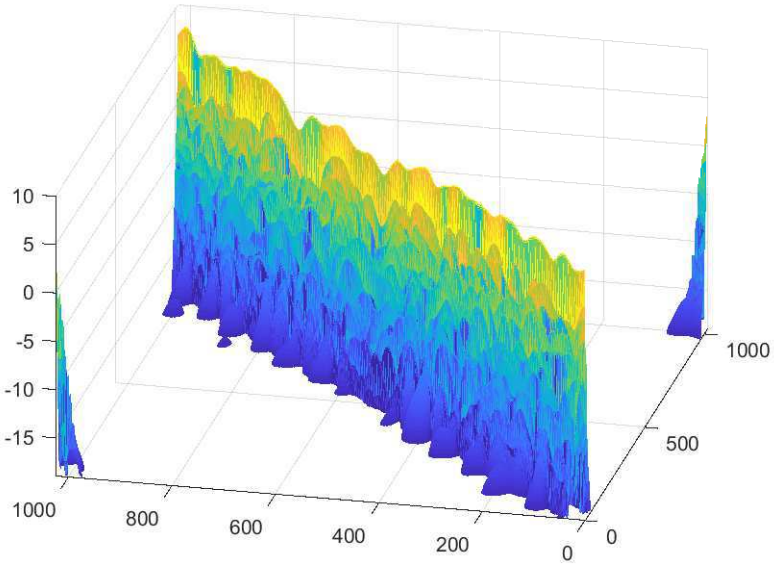

(b)

Figure 2.8: **R**-matrix for correlated fading. Figure 2.8(a): matrix **R** for one hydrophone., Figure 2.8(b): matrix **R** for the SIMO system for $A = 1$, which would be a heavy sea state. The transmitter is at 30 m and five hydrophones are between 30 m and 31.5 m depth.

A given transmit frequency f_c experiences a frequency shift of $a(t)f_c$, and we define the rms Mach number by a_{rms}. The rms doppler spread of the carrier frequency f_c is therefore $a_{\text{rms}}f_c$. We normalize this by our system symbol frequency to obtain

$$A = \frac{a_{\text{rms}}f_c}{f_{\text{sym}}} = a_{\text{rms}}f_c NT_s\,. \tag{2.7}$$

Typical values for A are in the range of $[0.005, 1]$, approximated by

$$A \approx \frac{v_{\text{rms}}f_c NT_s \times \text{depth}}{c \times \text{TX-RX distance}}\,. \tag{2.8}$$

Chapter 3

Single-Input Single-Output system (SISO)

In this chapter we study a single-input single-output transceiver and explain each part of the system in detail. The iterative demodulation technique is also discussed. Finally, we show the performance of the system.

3.1 Modulation and Demodulation

At the transmitter, encoded bits pass through a DQPSK or QPSK block which modulates the input signal using differential phase-shift keying (PSK). Then, the modulated symbols enter an inverse Fast Fourier Transform (iFFT) and a cyclic prefix (CP) is appended to the output sequence. At the receiver, after the CP is removed the FFT will be computed and the output signal passes through DQPSK or QPSK demodulation. This thesis will focus on coherent QPSK.

3.1.1 Log-Likelihood (LLR) Calculation

We begin with the calculation of the LLR computation for BPSK-modulated signal, and then we extend the model to QPSK modulation. First, let

$$y = \mu b + n \tag{3.1}$$

where $b = \pm 1$, $\mu = \sqrt{E_s} = \sqrt{E_b}$ and n is $\mathcal{N}(0, \sigma^2)$. The LLR for this received signal is given as

$$\text{LLR} = \log\left(\frac{\Pr(y|b=+1)}{\Pr(y|b=-1)}\right) = \log\left(\frac{\exp(y+\mu)^2/2\sigma^2}{\exp(y-\mu)^2/2\sigma^2}\right) = \frac{2\mu}{\sigma^2}y\,. \tag{3.2}$$

For one-dimensional signals $\sigma^2 = N_0/2$, so we also write

$$\text{LLR}(y) = \frac{4\sqrt{E_s}}{N_0}y = \frac{4\sqrt{E_b}}{N_0}y. \tag{3.3}$$

For Gray-coded QPSK, there are two bits for each symbol. Therefore, for a received

complex sample $y = y_0 + y_1 i = \mu x + n = \mu(b_0 + b_1 i) + n$, where b_0 and b_1 are ± 1, and $mu = \sqrt{2}/2$. The LLRs of the individual bits are calculated using the following symbol numbering:

Binary Gray-Code $b_0 b_1$	00	01	11	10
Complex QPSK Symbol	$\frac{\sqrt{2}}{2} + i\frac{\sqrt{2}}{2}$	$-\frac{\sqrt{2}}{2} + i\frac{\sqrt{2}}{2}$	$-\frac{\sqrt{2}}{2} - i\frac{\sqrt{2}}{2}$	$\frac{\sqrt{2}}{2} + i\frac{\sqrt{2}}{2}$
Symbol Number	0	1	2	3

The LLR of bit b_0 is computed as, keeping in mind that the complex signal noise variance equals N_0, that is, $N_0/2$ in each dimension:

$$\begin{aligned} \Lambda(b_0) &= \ln \frac{p(y|2) + p(y|3)}{p(y|0) + p(y|1)} \\ &= \ln \frac{\exp(-(y_0 - \mu)^2/N_0)}{\exp(-(y_0 + \mu)^2/N_0)} = \frac{4\mu}{N_0} y_0 \,. \end{aligned} \tag{3.4}$$

Since $E_s = 2E_b = 1$, we have $\mu = \sqrt{E_b}$, and

$$\Lambda(b_0) = \frac{4\sqrt{E_b}}{N_0}\, y_0 = \frac{2\sqrt{2}}{N_0}\, y_0; \qquad \Lambda(b_1) = \frac{4\sqrt{E_b}}{N_0}\, y_1 = \frac{2\sqrt{2}}{N_0}\, y_1 \,. \tag{3.5}$$

In our system the signal passes through the channel matrix $\mathbf{H}$ which consists of diagonal and off-diagonal elements as in (3.10). In this case, the variance of the noise in the denominator is aproximately the variance of the complex noise plus the variance of the interference that results from the off-diagonal elements of the channel matrix: $\sigma^2_{\text{tot}} = \sigma^2_{\text{noise}} + \sigma^2_I = N_0 + \sigma^2_I$.

The QPSK demodulation block in Figure 3.6 generates approximate LLR values according to

$$\Lambda(b) = -\frac{1}{\sigma^2_{\text{tot}}} \left(\min_{b=0} |x(b) - y|^2 - \min_{b=1} |x(b) - y|^2 \right) . \tag{3.6}$$

This basic equation needs to be adjusted to the matched-filter channel from (3.10) by realizing that the noise samples ψ_i are both correlated and weighted. They have the variance

$$E\left[\psi_i^* \psi_i\right] = R_{ii} \sigma^2_{\text{tot}} \,. \tag{3.7}$$

The LLR's across the N OFDM frequencies are then computed such that the i-th symbol LL's are given by

$$\begin{aligned}\Lambda(b) &= -\frac{1}{R_{ii}\sigma_{\text{tot}}^2}\left(\min_{b=0}|R_{ii}x(b)-y|^2-\min_{b=1}|R_{ii}x(b)-y|^2\right)\\ &= -\frac{R_{ii}}{\sigma_{\text{tot}}^2}\left(\min_{x(b=0)}\left|x(b)-\frac{y}{R_{ii}}\right|^2-\min_{x(b=1)}\left|x(b)-\frac{y}{R_{ii}}\right|^2\right). \qquad (3.8)\end{aligned}$$

This scaling of the LLRs is quite important. Furthermore, the total variance σ_{tot}^2 needs to be adjusted throughout the iterations. Currently this is done by subtracting the ideal received signal from the actual signal and computing the variance of the remaining noise and interference.

3.2 Repeat-Accumulate (RA) Codes

RA codes [2] can be viewed as a special type of serial turbo codes. As turbo codes they are the serial concatenation of two very simple component codes.

Figure 3.1 shows a block diagram of a non-systematic repeat accumulate encoder in serial concatenated form. The outer encoder is a simple repetition code with rate $R = 1/q$ and the inner encoder is a rate-one recursive encoder with feedback polynomical $1 + D$, that is, an accumulator. The inner and outer encoders are separated by the interleaver, and the overall code rate is $R = 1/q$. Despite their apparent simplicity, these codes perform very well, and for large block lengths and rates $R = 1/q \leq 1/3$, they have thresholds within 1 dB of the Shannon limit of the AWGN channel. The overall code rate of this family of codes is $R = r/(r + q)$ [2].

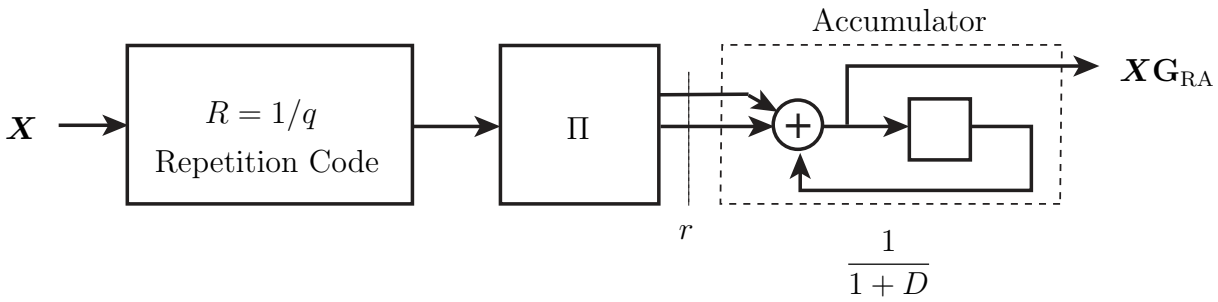

Figure 3.1: Block diagram of a repeat-accumulate code encoder.

A second type of codes are simple repetition codes, that is, the same structure as the RA code above, however, without the accumulator part. The interleaver is still there and required in order to operate the iterative cancelation loop[6].

3.3 The Matched-Filter Interference Channel

The received signal is first passed through a channel matched filter ,i.e.,

$$\boldsymbol{Y}_{\mathrm{mf}} = \mathbf{H}^H \boldsymbol{Y} = \mathbf{H}^H \mathbf{H} \boldsymbol{X} + \mathbf{H}^H \boldsymbol{\Psi} = \mathbf{R} \boldsymbol{X} + \boldsymbol{\Psi}' \tag{3.9}$$

where $\boldsymbol{Y}_{\mathrm{mf}}$ is the received signal after matched filtering, $\mathbf{R} = \mathbf{H}\mathbf{H}^H$ is the frequency-domain correlation matrix and $\boldsymbol{\Psi}' = \mathbf{H}^H \boldsymbol{\Psi}$ is Gaussian noise $\sim \mathcal{N}(0, \sigma^2 \mathbf{R})$.

The i-th element of the received signal in (3.9) is given as

$$Y_{\mathrm{mf},i} = R_{ii} X_i + \sum_{j \neq i} R_{ij} X_i + \Psi_i \sqrt{R_{ii}}\,. \tag{3.10}$$

The purpose of the cancelation loop is to remove the off-diagonal interfering terms through iterated subtraction. This is the essence of "turbo equalization", applied here to the ICI frequency-domain acoustic channel.

The inner loop of the receiver in Figure 3.7 contains a soft-output decoder, be that an LDPC, or a repetition code decoder. There are two scaling operations that take place in the inner loop: (i) The LLR scaling before and after the soft-output QPSK demodulator takes account of the diagonal gain values of the channel $\mathbf{R}$. (ii) The second scaling occurs at the input to the interleaver, where the LLR values are computed using the *exact* signal-to-noise and interference ratio (SINR), which is computed using the actual transmitted signal. Final designs will have to estimate this value, since the transmitted signal is naturally not available at the receiver.

In the following, Figure 3.2 shows the bit error rate curves of the repetition coded system before adding iterative demodulation. This system is unstable for time-varying environments.

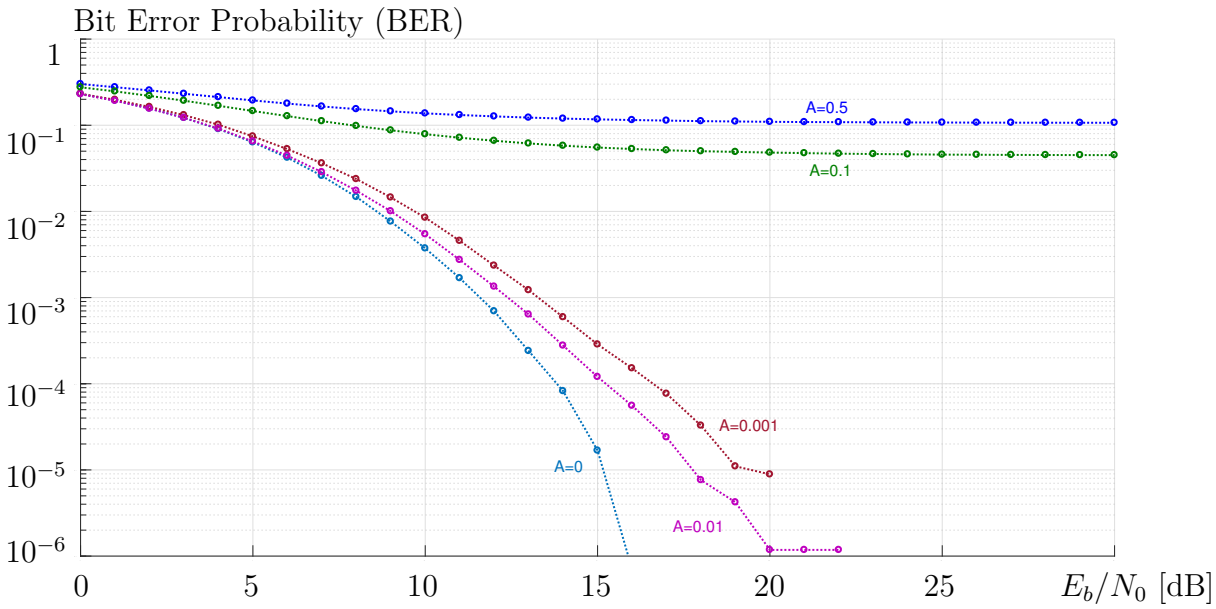

Figure 3.2: Repetition-coded BER curves for the dynamic and static ISI channels.

3.4 Iterative Demodulation

We use iterative cancelation methods to control the ICI that is generated by the time selectivity of the channel, first proposed for multi-user interference resolution. In the following, the structure of the iterative receiver will be described. The hydrophones and pre-amplifier in the receive array pass the signal through a channel-matched filter. The process requires that the channel is known. The output of the matched filter, $\mathbf{Y}_{\mathrm{MF}}$ is then given as $\boldsymbol{Y}_{\mathrm{MF}} = \mathbf{R}\boldsymbol{X} + \boldsymbol{\Psi}'$ where $\mathbf{R} = \mathbf{H}^H\mathbf{H}$ and $\boldsymbol{\Psi}'$ is the colored noise, resulting from this operation. We also define the matrices of the diagonal and off-diagonal components of $\mathbf{R}$ as

$$\mathbf{D} = \mathrm{diag}(\mathbf{R}); \qquad \mathbf{R}_{\mathrm{off}} = \mathbf{R} - \mathbf{D}. \tag{3.11}$$

The iterative receiver consists of demapping, soft decoding and, soft remapping. The received signal from the matched filter passes through the demodulator and is

decoded by the soft decoder. Then, the soft symbols produced by the decoder are remapped and used to generate the signal $\tilde{\boldsymbol{X}}$ which is a local replica of the transmitted signal $\boldsymbol{X}$. In case of QPSK symbols the real and imaginary components of the N-dimensional vector of QPSK symbols form a $2N$-dimensional vector which is processed by the soft decoder. We will call the de-mapping, error correction decoding, and soft re-mapping block the *decoder* for simplicity. The decoder outputs soft bit estimates which are used to form the vector $\tilde{\boldsymbol{X}}^{(i)}$ of newly estimated soft QPSK symbols at iteration i.

The interference cancellation block computes

$$\boldsymbol{Y}_{\mathrm{MF}}^{(i)} = \boldsymbol{Y}^{(i)} - \mathbf{R}_{\mathrm{off}}\tilde{\boldsymbol{X}}^{(i)} = \mathbf{R}\boldsymbol{X} + \boldsymbol{\Psi}' - \mathbf{R}_{\mathrm{off}}\tilde{\boldsymbol{X}}^{(i)} = \mathbf{D}\boldsymbol{X} + \mathbf{R}_{\mathrm{off}}(\boldsymbol{X} - \tilde{\boldsymbol{X}}^{(i)}) + \boldsymbol{\Psi}' \quad (3.12)$$

where i represents the iteration index. In (3.12), the first term $\mathbf{D}\boldsymbol{X}$ provides us with the ICI-free signal where as the second term is the residual interference term from the off-diagonal components. The initialization of the iterative process starts from the first iteration when the decoder operates on the received matched filtered vector $\boldsymbol{Y}^{(i)}$ to produce the first soft-symbol vector $\boldsymbol{Y}^{(i)}\tilde{X}^{(1)}$.Since we experienced some difficulties with the original LDPC code in the iterative system, we also built a system based on repetition coding. This system has a lower coding rate and is more robust to the fading events that caused the high-rate LDPC code to fail for highly dynamic channels with $a > 0.1$.

3.5 Simulation Examples

Simulations were run for two coding systems: (i) The high-rate (6,32) IEEE 802.3an LDPC code, and, (ii) a low-rate repetition coding system. Both coding strategies are optimal in the limit, as explored in [6]. Figure 3.3 shows the performance of the LDPC coding system on various static channels, that is, channels without time-selectivity, and therefore without ICI. The curves AWGN QPSK and AWGN DQPSK are the reference BER performance of the code over additive Gaussian noise channels with and without differential modulation. The various static BER curves refer to the ISI channel discussed in Figure 2.2. Due to the strong ISI nature, it is evident that the matched filter is necessary for adequate performance. Using a channel-matched filter, of course, requires knowledge of the channel!

Figure 3.4, on the other hand, shows the performance of the LDPC-coded system over dynamic channels, that is, over channels with a non-zero Mach number a. We note that the performance of the system is very good and essentially equivalent to the static performance up to Mach numbers of about $a \approx 0.01$. For larger Mach numbers,, the performance quickly decays. The primary suspect of the code's inability to handle larger Mach numbers, despite full knowledge of the channel frequency response matrix $\mathbf{H}^{(f)}$ is that this specialized code is very sensitive to outages that occur as a result multipath fading, see Figure 2.3.

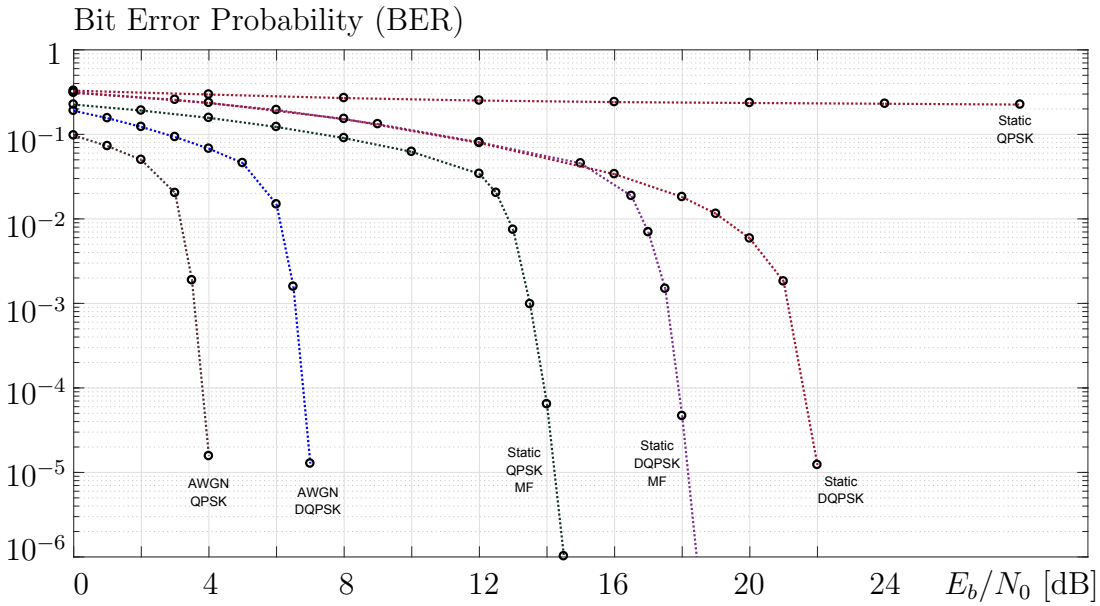

Figure 3.3: LDPC-coded BER curves for the static ISI test channel.

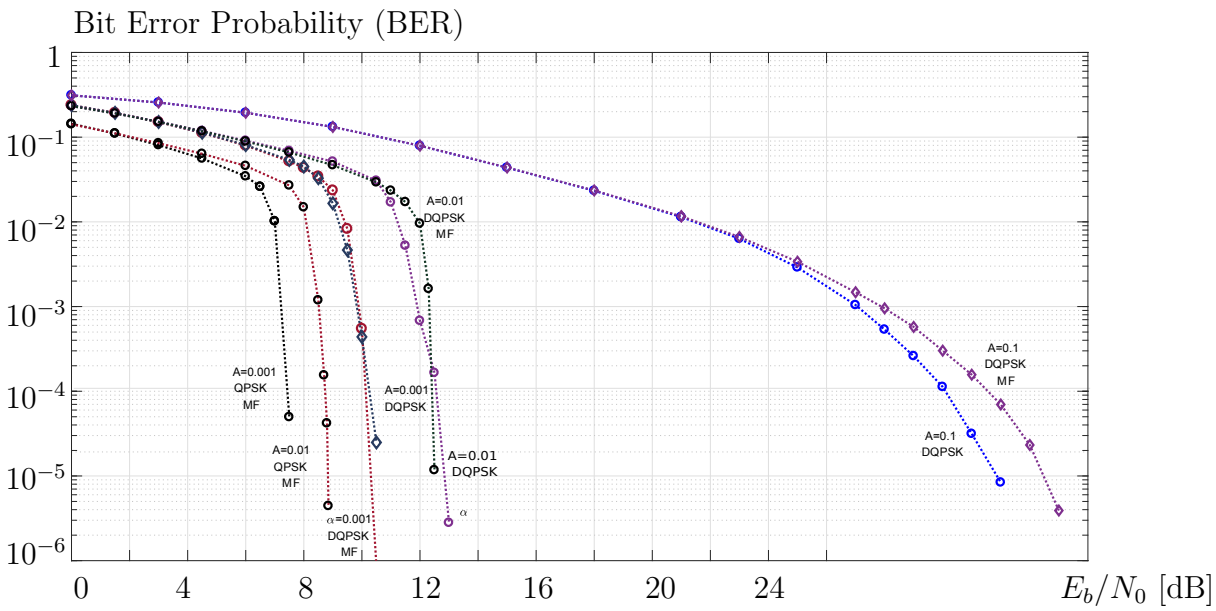

Figure 3.4: LDPC-coded BER curves for the dynamic ISI channel with $A = 0.01$.

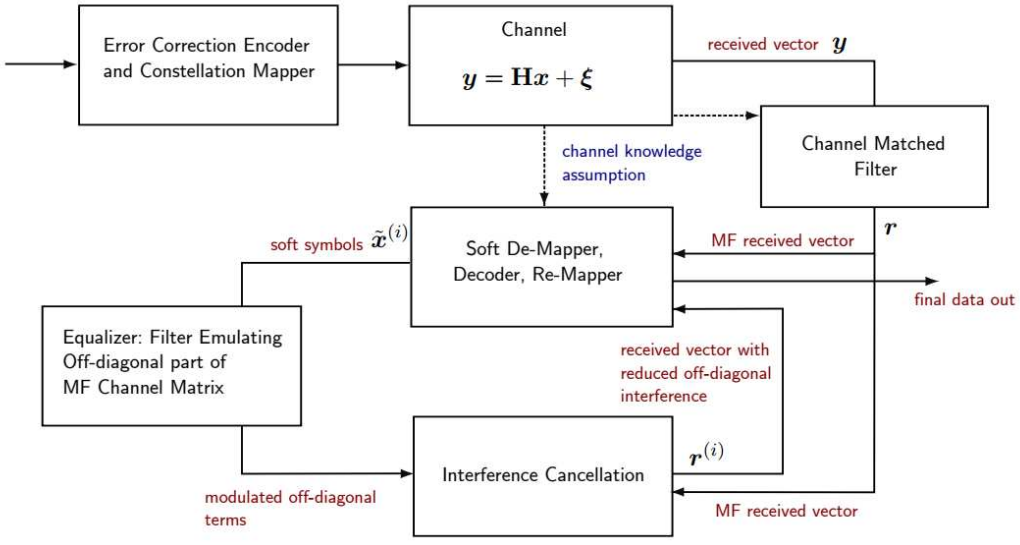

Figure 3.5: Iterative cancelation and decoding loop [7].

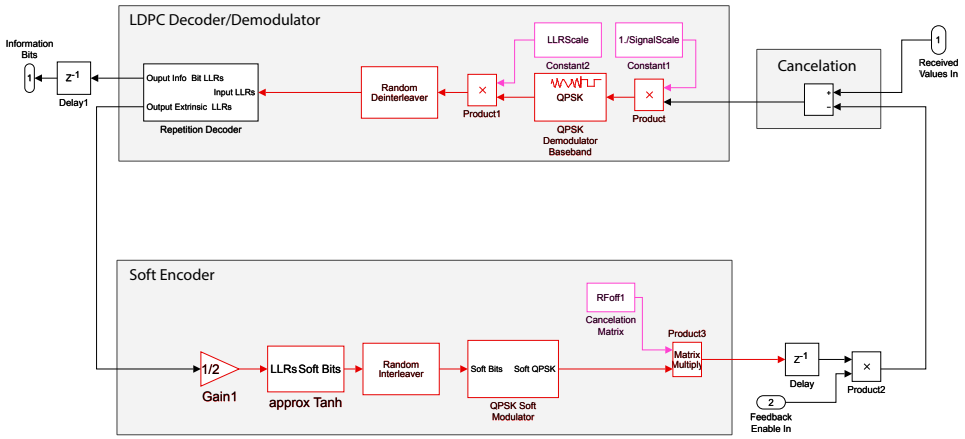

Figure 3.6: Iterative cancelation and decoding loop consisting of soft-decision error control decoding and soft symbol re-generation.

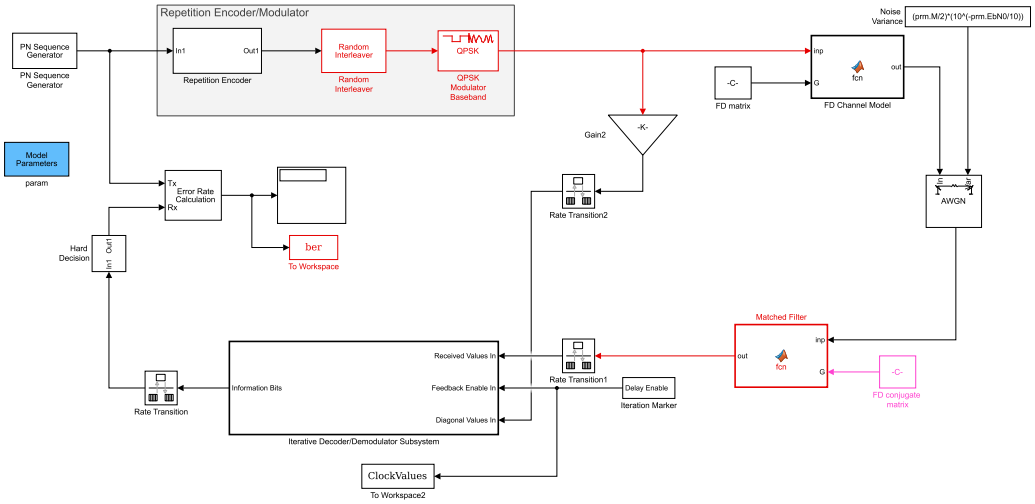

Figure 3.7: Iterative cancelation system using a repetition coded system. The Simulink file name is `Semi_FullOFDM_Rep_Iterative.xls`. The different colors indicate different timing domains: Green runs at the transmit rate T_f, red operates at the iteration rate $T_I = T_f/I$.

Chapter 4

Single-Input Multiple-Output (SIMO)

In order to increase the transmission rate and enhance detection perfomance, we increase the number of hydrophones. Figure 4.1 shows that, at the receiver side, the received signal is combined whereby each of the received signals goes through its corresponding matched filter preprocessor and then the sum of these output signals is delivered to the receiver.

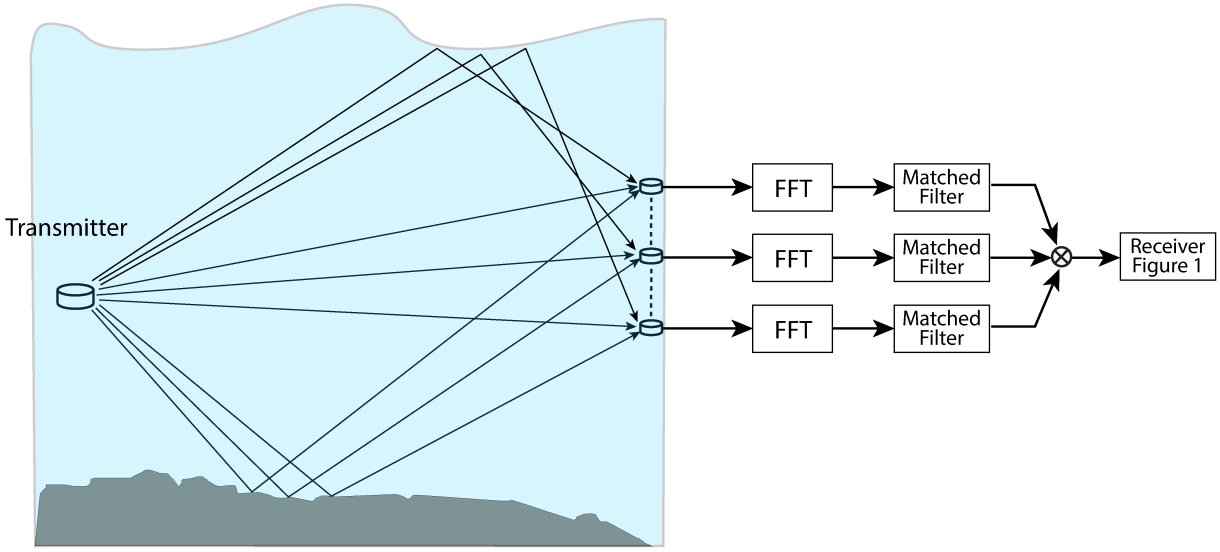

Figure 4.1: Illustration of a multiple-hydrophone receiver and front-end maximum-ratio combining, which amounts to receiver beam-forming for maximum received power.

Given that there are N_h hydrophones, there are then also N_h preprocessing chains consisting of FFT processors and matrix matched filters. Mathematically we write for the received signal at each hydrophone

$$\boldsymbol{Y}_{\mathrm{MF},k} = \mathbf{R}_k \boldsymbol{X} + \boldsymbol{\Psi}'_k \,. \tag{4.1}$$

The signal that enters our iterative receiver is then the linear combination of the individual signal streams, and we obtain for the i-th iteration

$$\boldsymbol{Y}_{\mathrm{MF}}^{(i)} = \sum_{k=1}^{N_h} \mathbf{Y}_{\mathrm{MF},k}^{(i)} = \sum_{k=1}^{N_h} \mathbf{R}_k^{(i)} \boldsymbol{X} + \boldsymbol{\Psi} = \sum_{k=1}^{N_h} \mathbf{Y}_{\mathrm{MF},k}^{(i)} - \sum_{k=1}^{N_h} \mathbf{R}_{\mathrm{off,k}} \tilde{\boldsymbol{X}}^{(i)} + \boldsymbol{\Psi} \tag{4.2}$$

where the individual noise terms combine into a noise term $\boldsymbol{\Psi}$ which has N_h times the power of each individual noise term. Further we write

$$\begin{aligned} \boldsymbol{Y}_{\mathrm{MF}}^{(i)} &= \sum_{k=1}^{N_H} \mathbf{R}_k \boldsymbol{X} - \sum_{k=1}^{N_H} \mathbf{R}_{\mathrm{off,k}} \tilde{\boldsymbol{X}}^{(i)} + \boldsymbol{\Psi} = \sum_{k=1}^{N_H} (\mathbf{D_k} + \mathbf{R}_{\mathrm{off,k}}) \boldsymbol{X} - \sum_{k=1}^{N_H} \mathbf{R}_{\mathrm{off,k}} \tilde{\boldsymbol{X}}^{(i)} + \boldsymbol{\Psi} \\ &= \sum_{k=1}^{N_H} \mathbf{D_k} \boldsymbol{X} + \sum_{k=1}^{N_H} \tilde{\mathbf{R}}_k \left(\boldsymbol{X} - \tilde{\boldsymbol{X}}^{(i)} \right) + \boldsymbol{\Psi} \,. \end{aligned} \tag{4.3}$$

While the iterative receiver only requires knowledge of the combined correlation matrix $\mathbf{R} = \sum_{k=1}^{N_H} \mathbf{R}_k$, the preprocessors will require knowledge of the individual matrices $\mathbf{R}_k$, which therefore will all need to be estimated separately.

The operation in (4.3), as discussed above, effects maximum-ratio combining of the received signals at the different hydrophones.

4.1 Receiver Operation

The output signal after the matched filter of the k-th receive hydrophone chain is given by (4.1). The maximum-ratio-combined received signal goes through the cancellation and iterative decoding/demodulation block. Equations 4.2 and 4.3 show the signal after the i-th iteration in the cancellation step. The first term in 4.3 is the signal term we are interested in, i.e., the self-correlated data signals on the diagonal. The second term is the residual interference term from the off-diagonal ICI components and the last term is channel noise.

Figure 4.2 shows the iteration variance evolution of the iterative receiver as a function of the iterations. If the SNR is too small, or the interference too large, certain higher-rate codes fail to converge. We will investigate this threshold point quantitatively in future work.

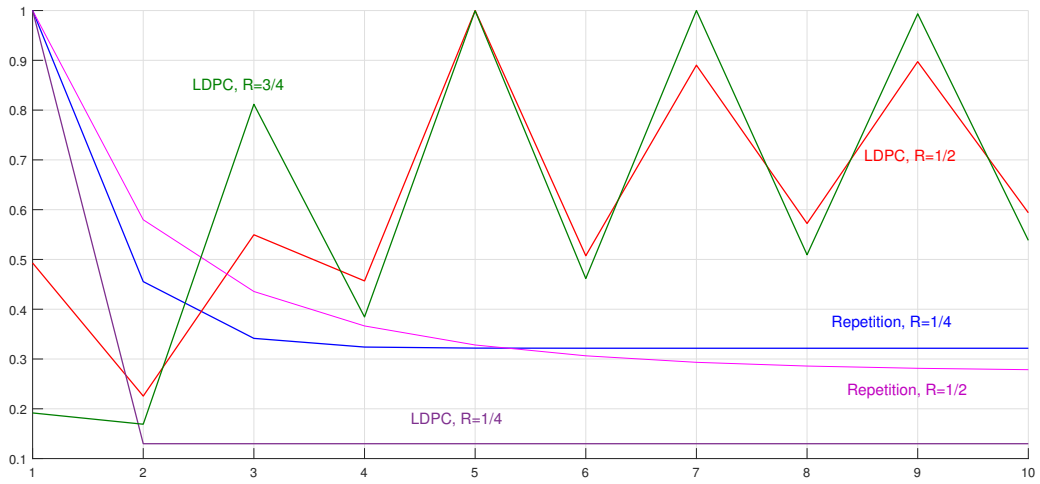

Figure 4.2: Normalized iteration variance of a SIMO system versus the number of iterations. The transmitter located at 10 m and five hydrophones at 10 m to 11.48 m. $A = 1$ and $E_b/N_0 = 7$ dB.

We observe that as long as the system can converge, it will do so quite rapidly within a few iterations. The repetition codes system appears to be more robust, which is a natural consequence of its interference resiliences [6].

4.2 Capacity Calculation

For any multiple-input multiple-output (MIMO) channels, which includes our OFDM channels, the linear channel mixing matrix $\mathbf{H}$ can be decomposed via the *singular value decomposition* (SVD) into the product

$$\mathbf{H} = \mathbf{U}\mathbf{\Sigma}\mathbf{V}^H$$

where $\mathbf{U} \in \mathbb{C}^{N_r \times N_r}$ and $\mathbf{V} \in \mathbb{C}^{N_t \times N_t}$ are *unitary matrices*, i.e., $\mathbf{U}\mathbf{U}^H = \mathbf{U}^H\mathbf{U} = \mathbf{I}_{N_r}$, and $\mathbf{V}\mathbf{V}^H = \mathbf{V}^H\mathbf{V} = \mathbf{I}_{N_t}$. The matrix $\mathbf{\Sigma} \in \mathbb{C}^{N_r \times N_t}$ contains the singular values $\{\sigma_s, s = 1, \ldots, S\}$ of $\mathbf{H}$ on its diagonal, which are the positive square roots of the nonnegative eigenvalues of $\mathbf{H}\mathbf{H}^H$ or $\mathbf{H}^H\mathbf{H}$. Note that $\mathbf{\Sigma}$ may not be a square matrix, which simply means that the number of nonzero singular values can be no larger than the minimum dimension of $\mathbf{H}$, and is in fact equal to its rank.

The overall rate in the system, which is obtained for the Gaussian–distributed input symbols, is given by

$$R = \sum_s R_s = \sum_{s=1}^{S} \log_2 \left(1 + \frac{\sigma_s^2 P_s}{N_0}\right) \tag{4.4}$$

but requires that the channel is known at the transmitter. Henceforth we use the variables $\lambda_s = \sigma_s^2$ for the powers of the different *eigen modes*. In order to use the above equation, the colored noise in (4.1) needs to be converted to white noise. Accordingly, we have

$$\begin{aligned} \mathrm{E}[\boldsymbol{\Psi}'\boldsymbol{\Psi}'^H] &= \mathrm{E}\left[\sum_k \mathbf{H}_k^H \boldsymbol{\Psi}_k \sum_{k'} \boldsymbol{\Psi}^H \mathbf{H}_{k'}\right] = \sum_k \mathbf{H}_k^H \mathrm{E}\left[\boldsymbol{\Psi}\boldsymbol{\Psi}^H\right] \mathbf{H}_k \\ &= \sigma^2 \sum_k \mathbf{H}_k^H \mathbf{H}_k = \sigma^2 \sum_k \mathbf{R}_k = \sigma^2 \mathbf{R} = \sigma^2 \mathbf{C}^H \mathbf{C} \end{aligned} \tag{4.5}$$

where $\sigma^2 = N_0/2$, $\mathbf{R} = \mathbf{C}^H\mathbf{C}$, $\mathbf{C} = U_R\sqrt{\Sigma_R}$, and from the SVD decomposition, $\mathbf{R} = \mathbf{U}_R\boldsymbol{\Sigma}_R\mathbf{V}_R$. As a result, noise can be whitened by

$$\begin{aligned} \mathbf{C}^{-1}\boldsymbol{Y}_{\mathrm{MF}} &= \mathbf{C}^{-1}\mathbf{R}\mathbf{X} + \mathbf{C}^{-1}\boldsymbol{\Psi}' \\ \boldsymbol{Y}' &= \mathbf{C}^{-1}\mathbf{R}\boldsymbol{X} + \sigma\mathcal{N}(0, \mathbf{I}) \end{aligned} \tag{4.6}$$

where $\mathbf{I}$ is an identity matrix. Therefore, in (4.4) σ_s^2 are the singular values of $\mathbf{H} = \mathbf{C}^{-1}\mathbf{R}$.

Moreover, P_s in (4.4) is the power allocated to the different eigen modes s, in such a way that that $P_s \triangleq \mathrm{E}\left[|x_s[n]|^2\right]$, and the channel capacity is formally given by

$$C_{\mathrm{I}} = \max_{\substack{P_1,\ldots,P_S, \\ \sum_s P_s \le P}} \sum_{s=1}^{S} \log_2 \left(1 + \frac{\lambda_s P_s}{N_0}\right) \tag{4.7}$$

where the total power allocated to the eigenmodes is limited such that $\sum_s P_s \le P$. In the case, where the channel is not known at the transmitter–the usual case for acoustic system due to the fact that the roundtrip time typically exceeds the coherence time of the channel, we set $P_s = P/N$ where N is the number of subcarriers in on OFDM symbol.

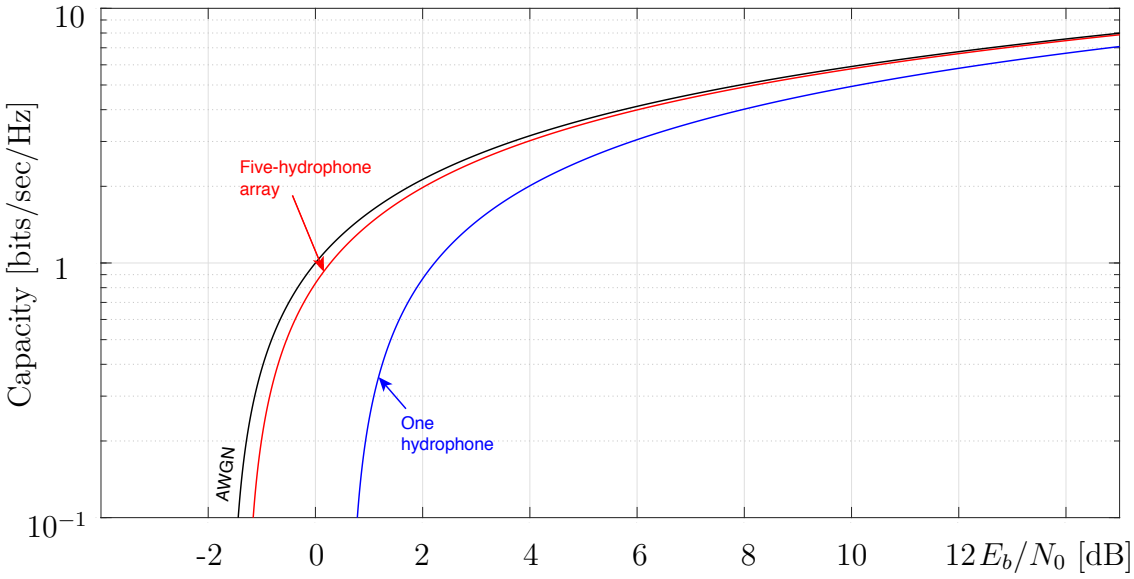

Figure 4.3: Capacity of the channel from Figure 2.7 with uncorrelated fading with Doppler effect: $A = 1$. The transmitter is at 30 m and five hydrophones are between 30 m and 31.5 m.

The laws of large numbers states that the average of the results from a large number of trials is close to the expected value. Based on this law, as we increase the number of hydrophones, the sum of diagonal parts of channel matrices becomes close to the expected value of the channel diagonal part. Therefore, as the power of the each channel is normalized, the sum of **R**-matrices of these channels becomes flat. The performance of the flat channel with unit expected value is close to the AWGN channel. Consiquently, as Figure 4.3 shows, the capacity of SIMO channels is close to the AWGN channel in the uncorrelated fading scenario.

We can see from Figure 4.3 that even as few as $N_h = 5$ hyrdophones essentially transforms the channel into one with a capactiy close to that of an ideal AWGN channel. This is due to the diversity of $N \times N_h = 1024 \times 5$ channels. Moreover, compared with the curves in Figure 4.3, the capacity of the channels with correlated fading is less than uncorrelated fading, since in the correlated case we lose the channel diversity. Capacity results for the fully correlated channel are shown in Figure 4.4.

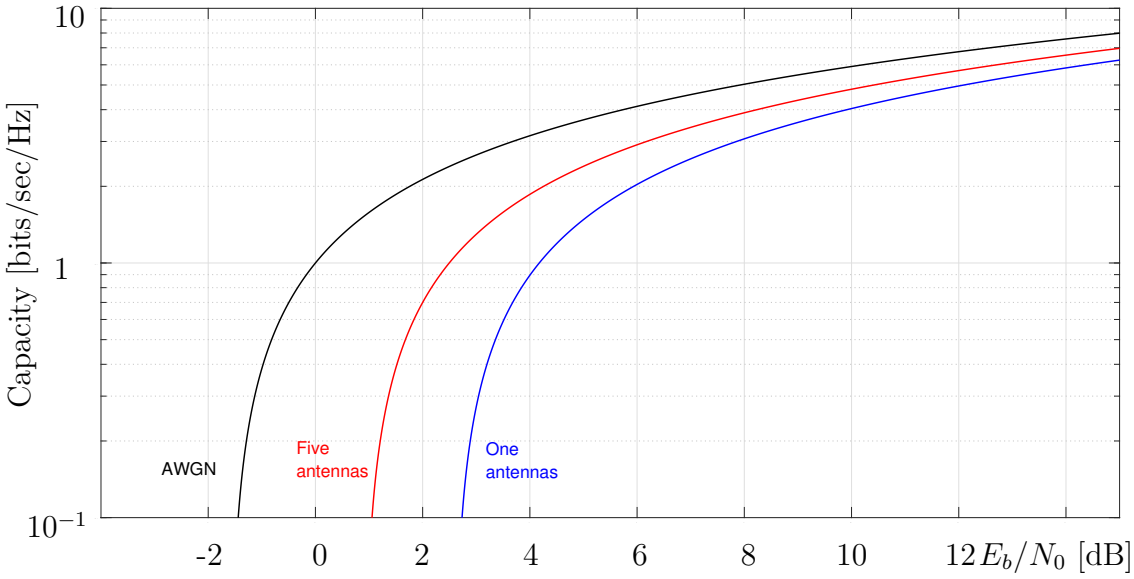

Figure 4.4: Capacity of the channel from Figure 2.8 with correlated fading, $A = 1$. The transmitter is at 30 m and five hydrophones are between 30 m and 31.48 m.

4.3 Simulation Results

In the following, we use two encoding methods to test the system: LDPC and repetition encoding. Both methods are near optimal for cancelation systems as explored in [6]. The bit error rate curves show that in the system with multiple hydrophones, the overall performance is better than that of a SISO system, even with when we normalize the received power. This is to be expected from Figures 4.3 and 4.4. Below we measure this improvement in the channel as the energy ratio of the diagonals of the matrix $\mathbf{R}$ over the off-diagonal elements are calculated for $a = 5$ and $a = 0.1$.

- $A = 5$ SISO: $\frac{\text{Power}_{diag}}{\text{Power}_{\text{Off-diag}}} = \frac{1}{11.74} = 0.085$ SIMO: $\frac{\text{Power}_{diag}}{\text{Power}_{\text{Off-diag}}} = \frac{5}{25.99} = 0.192$

- $A = 0.1$ SISO: $\frac{\text{Power}_{diag}}{\text{Power}_{\text{Off-diag}}} = \frac{1}{2.18} = 0.457$ SIMO: $\frac{\text{Power}_{diag}}{\text{Power}_{\text{Off-diag}}} = \frac{5}{5.83} = 0.857$

The bit error rates below show the performance of the system for different simulation scenarios. Figure 4.5 compares the BER of a system with repetition and LDPC coding and $A = 0$. The parameter A quantifies the Doppler effect of environment,

where $A = 0$ defines a (quasi-) stationary channel. Figure 4.6 shows the BER for different typical A values and uncorrelated fading, while the channel for Figure 4.7 has correlated fading.

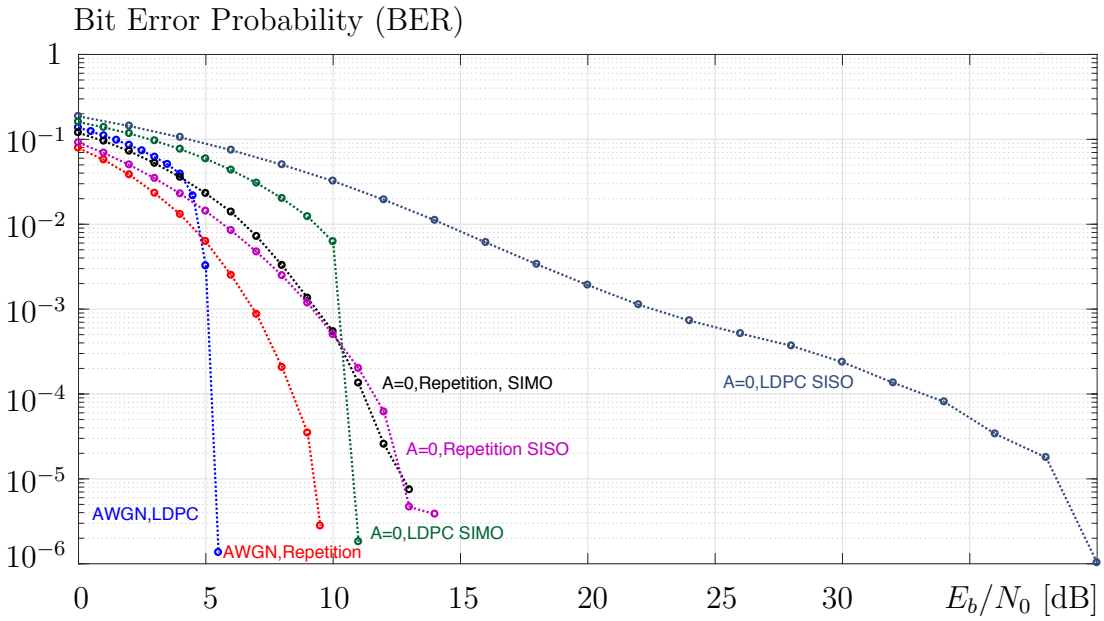

Figure 4.5: Bit error rates for the repetition coded system for AWGN and static channel. The transmitter is at 30 m and five hydrophones are between 30 m and 31.5 m.

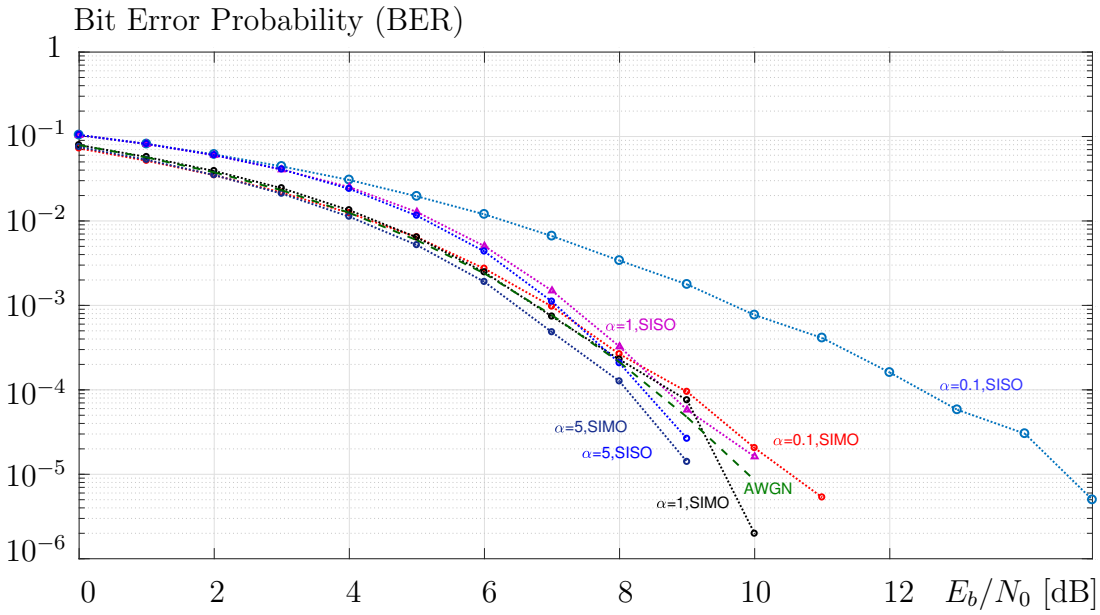

Figure 4.6: Bit error rates for the repetition coded system for *any* value of A and uncorrelated fading. The transmitter is at 30 m and five hydrophones are between 30 m and 31.5 m.

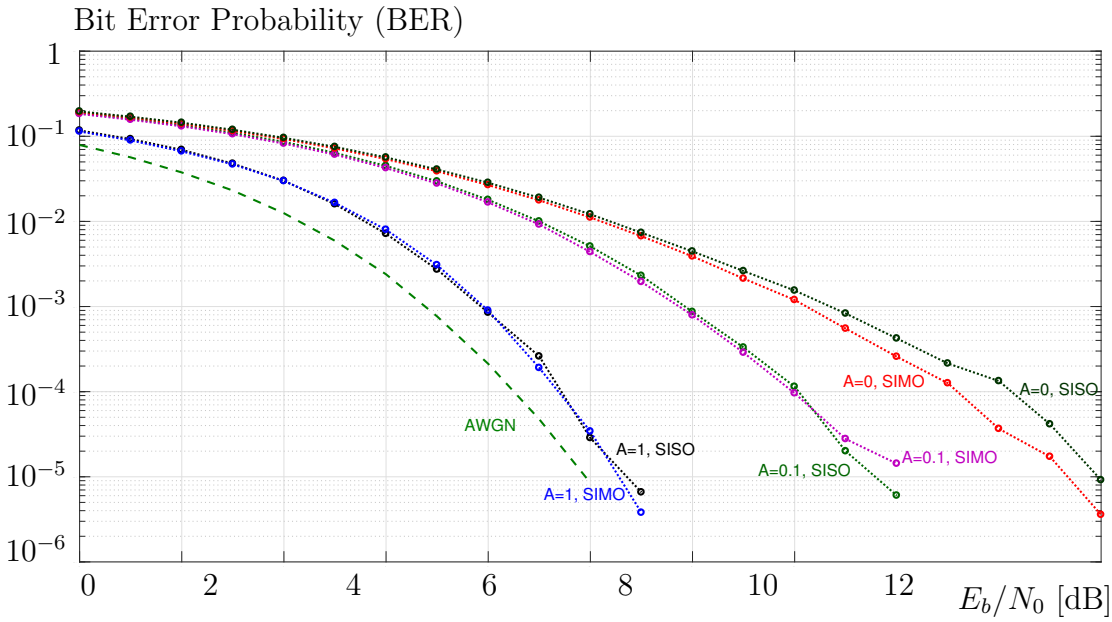

Figure 4.7: Bit error rates for the repetition coded system for several values of A and correlated fading. The transmitter is at 30 m and five hydrophones are between 30 m and 31.48 m.

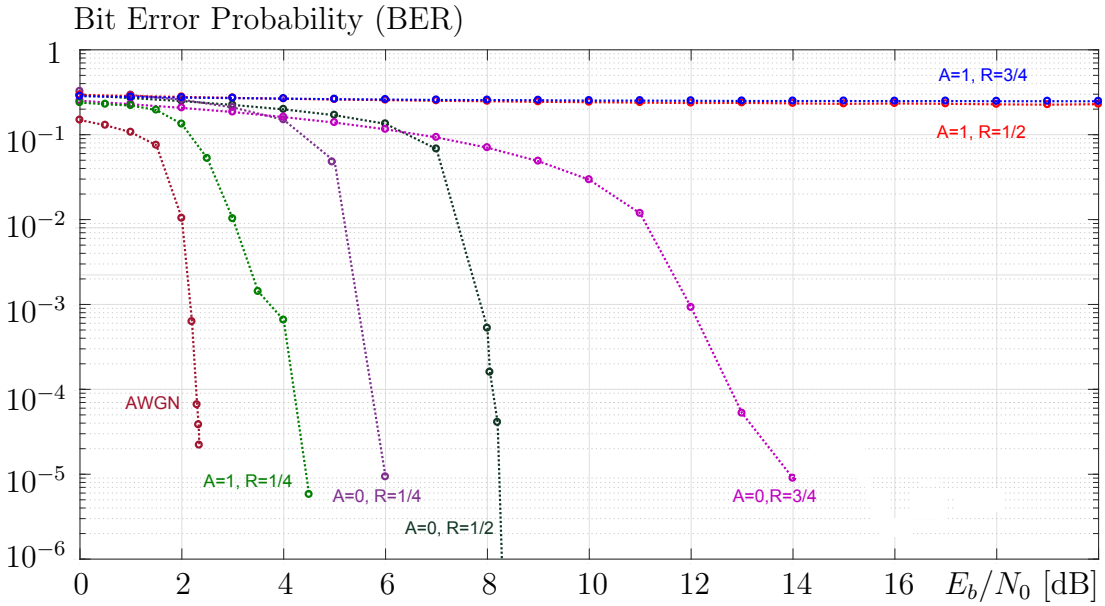

Figure 4.8: Bit error rates for the LDPC coded SIMO system with different rates and different correlated Doppler effects. The transmitter is at 30 m and five hydrophones are between 30 m and 31.48 m.

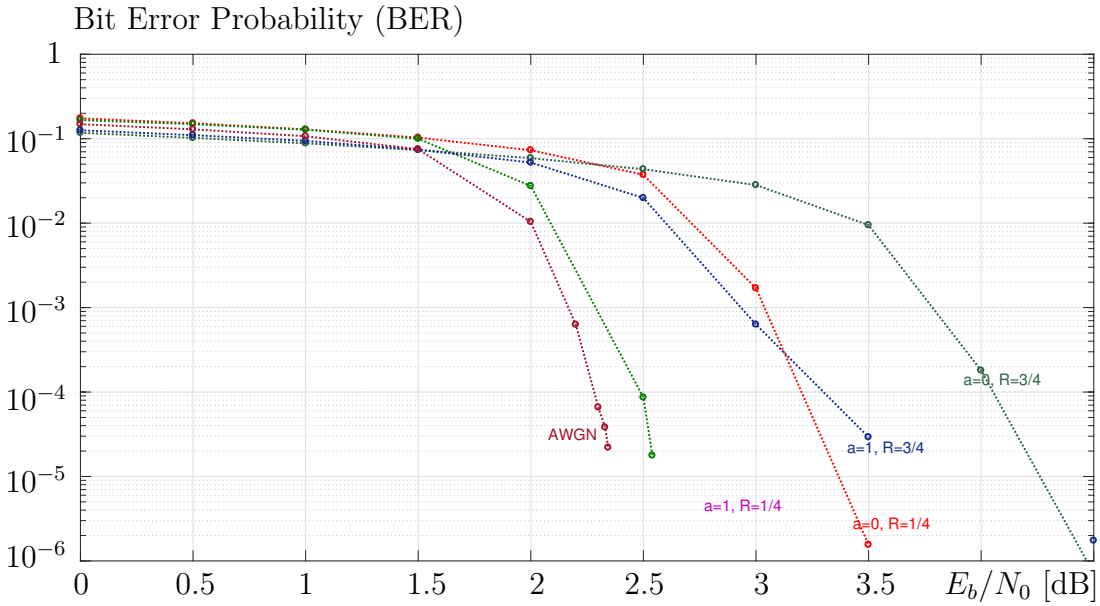

Figure 4.9: Bit error rates for the LDPC coded SIMO system with different rates and different uncorrelated Doppler effects. The transmitter is at 30 m and five hydrophones are between 30 m and 31.5 m.

Chapter 5

Multiple Transmissions

In order to increase the system rate, we may add more transmitters to the system. In the following we describe the performance of the system in the presence of other transmitters. The k-th transmitter's signal is given by

$$\boldsymbol{Y}_k = \sum_{j=1}^{N_u} \mathbf{H}_{jk}\boldsymbol{x}_j + \boldsymbol{\Psi} \tag{5.1}$$

where N_u is the number of users (transmitters). In order to detect the data from the j-th transmitter, we use a matched filter using $H_{jk}, k = 1, .., N_H$. The output of the matched filter is then given

$$\boldsymbol{Y}_{\mathrm{MF},j} = \sum_{k=1}^{N_H} \mathbf{H}'_{jk}\mathbf{H}_{jk}\boldsymbol{x}_j + \sum_{k}^{N_H}\sum_{l\neq j}^{N_u-1} \mathbf{H}'_{jk}\mathbf{H}_{lk}\boldsymbol{x}_l + \boldsymbol{\Psi}' \tag{5.2}$$

The output signal of each iteration of for the j-th user's signal is given

$$\boldsymbol{Y}^{(i)}_{\mathrm{MF},j} - \sum_{k=1}^{N_H} \mathbf{R}_{\mathrm{off}}\tilde{\boldsymbol{x}}^{(i)}_j - \sum_{k}^{N_H}\sum_{l\neq j}^{N_u-1} \mathbf{H}'_{jk}\mathbf{H}_{lk}\tilde{\boldsymbol{x}}^{(i)}_l + \boldsymbol{\Psi} \tag{5.3}$$

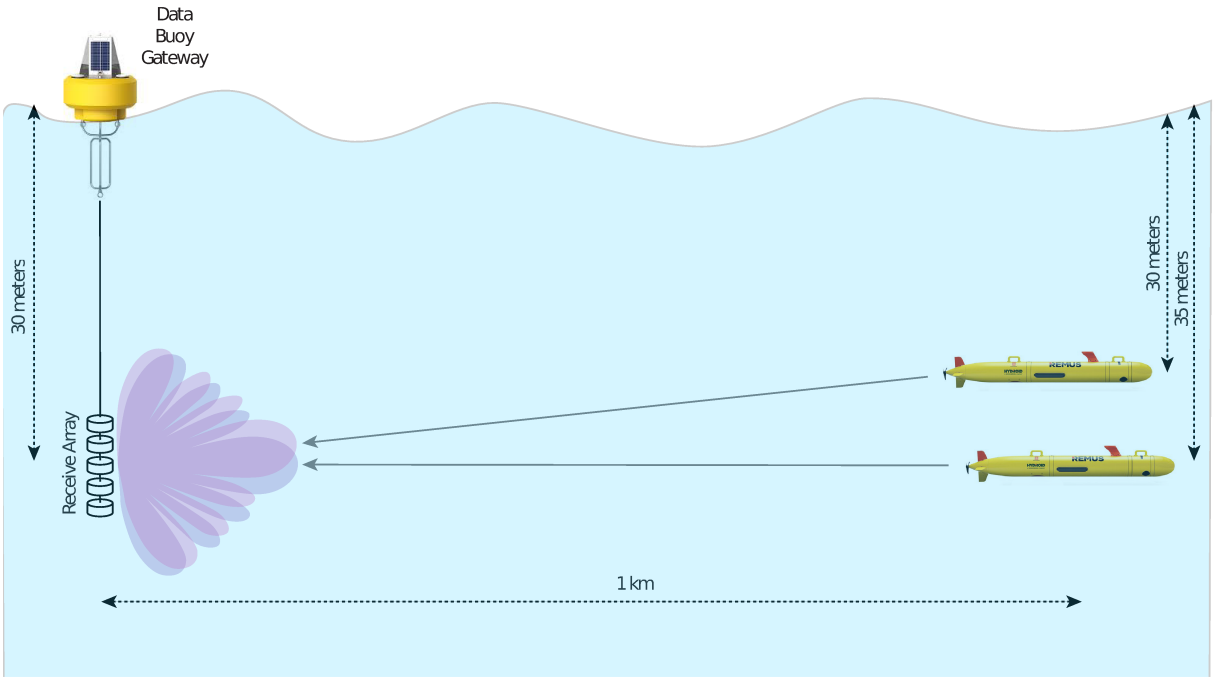

Figure 5.1: Iterative receiver discussed in this report.

where $\mathbf{R}_{\text{off}}$ contains the off-diagonal elements of matrix $\mathbf{H}'_{jk}\mathbf{H}_{jk}$. In (5.3), the second term is the unfavourable residual interchannel interference and the third term is the cross-interference from other users.

In this section we focus on studying the system with correlated channels. The signal-to-interference ratio (SIR) related to the channels in Figure 2.8 (correlated fading) are given by

- SISO: $\frac{\text{Power}_{diag}}{\text{Power}_{\text{Off-diag}}} = \frac{1}{6.19} = 0.161$ SIMO: $\frac{\text{Power}_{diag}}{\text{Power}_{\text{Off-diag}}} = \frac{5}{30.23} = 0.165$

Consequently, we notice that the signal combining at the receiver has only marginal impact on the dynamics of the channel, as measured by the power ratios above, and combining has the effect of gathering energy by steering the receive-array beam towards the signal of interest.

5.1 Simulation Results

Below we show the performance of a MIMO system for different channel types, correlated or uncorrelated fading, different transmitter distances, and different Doppler effects.

Figure 5.3 and 5.4 show that with an increase of the distance between users, the BER decreases, arguably because the channels become less similar, which allows the receiver a better separation of the transmissions.

Using the Bellhop software, we change the location of the transmitters and produce different channel models for different users. Figure 5.2 shows the channel delay profiles for 2 different users while they are transmitting to the same receiver.

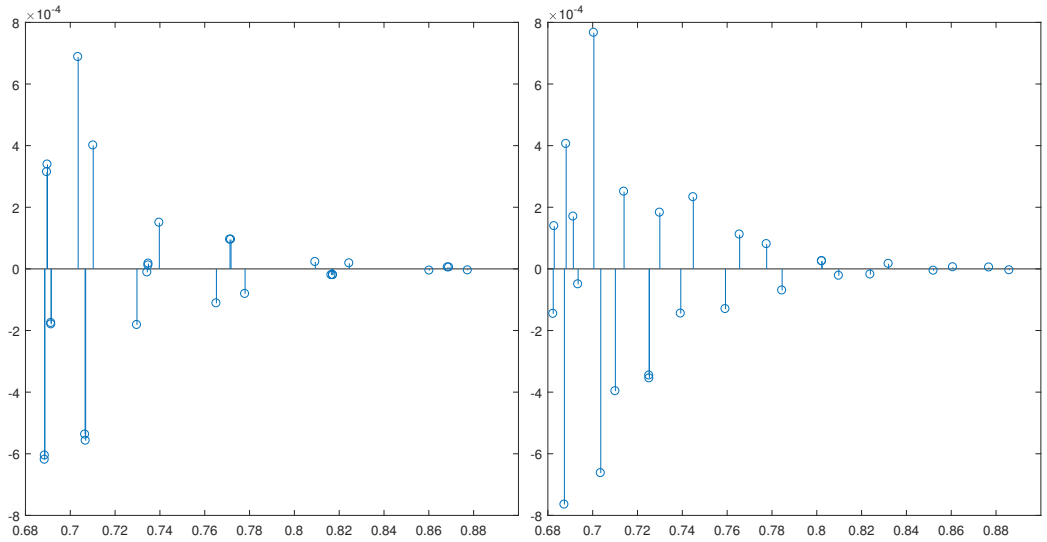

Figure 5.2: Channel delay profile for different location of transmitters. 5.2(a) is related to the transmitted located at 10 m from the sea floor and the transmitter of figure 5.2(b) is at 30 m.

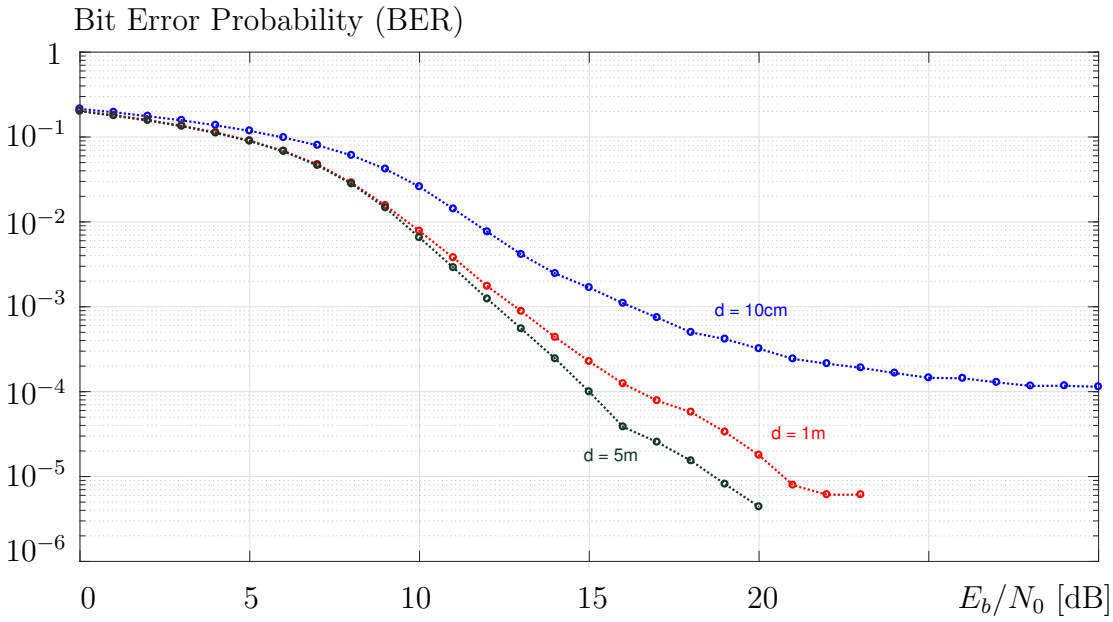

Figure 5.3: Bit error rates for the repetition coded system for several vertical distance of the first user from the second one. First user is located at 10 m and receiver at 10 m. $A = 1$ and the fading is correlated.

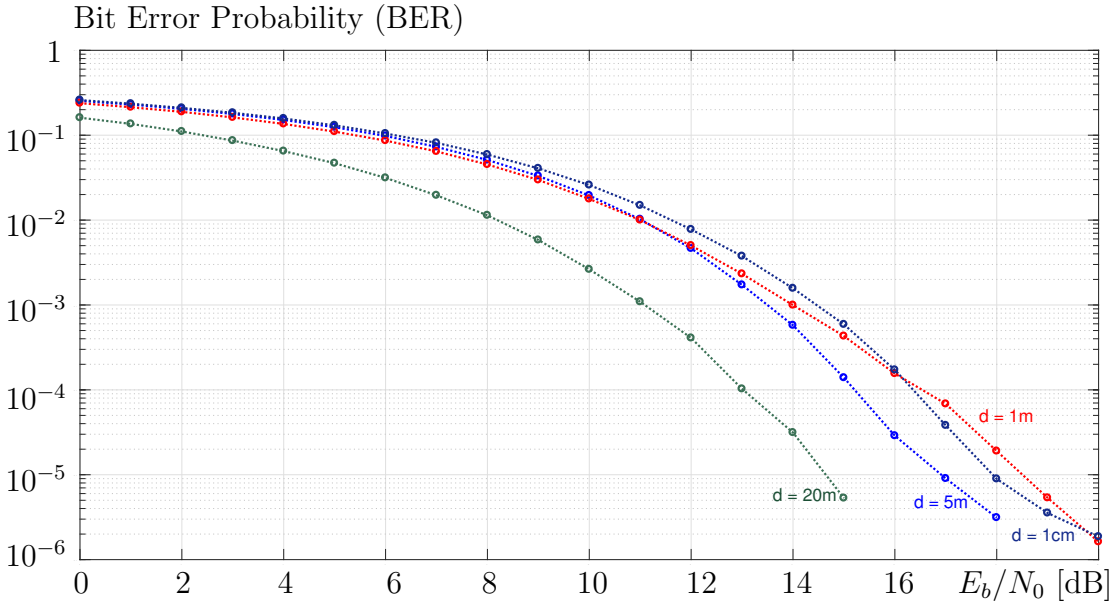

Figure 5.4: Bit error rates for the repetition coded system for several values of d of vertical distance between the two transmitters, and for $A = 0.5$ and uncorrelated fading. The first transmitter is at 30 m and receivers are between 30 m to 31.5 m.

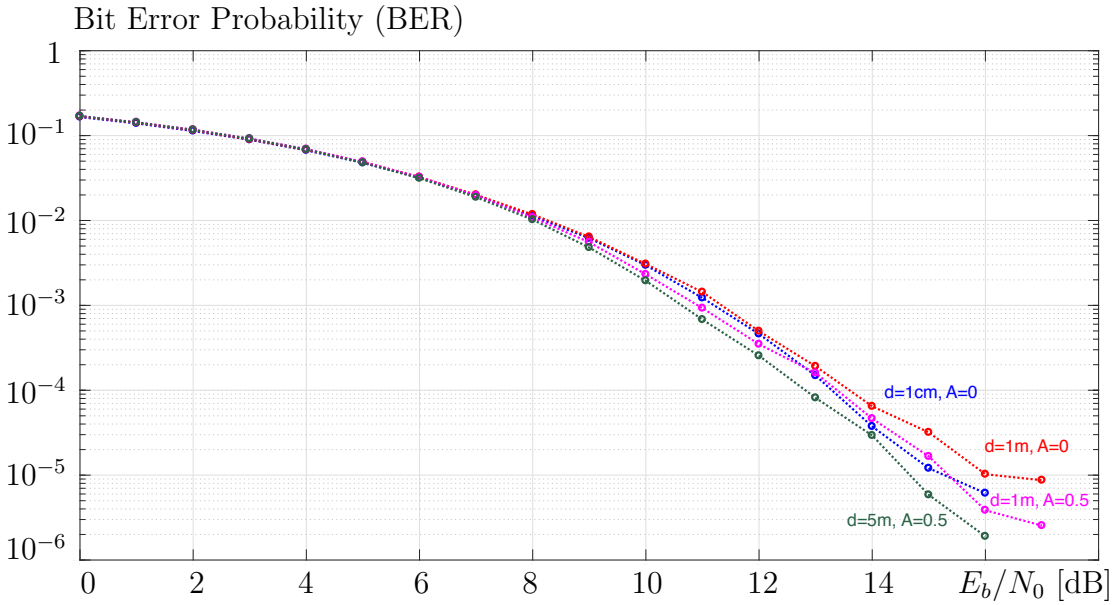

Figure 5.5: Bit error rates for the repetition coded system for different vertical distances between the transmitters and for different a's and uncorrelated fading. First user is located at 10 m and receive hydrophones are between 10 m and 11.48 m.

Chapter 6

Conclusion and Future Work

The purpose of this thesis was to introduce an OFDM system and its application for an underwater acoustic environment.The system assumed that the transmission channel is known. We used an LDPC and a low rate repetition coded system which equalized the channel. We implemented an iterative cancellation loop to cancel interference. In addition, instead of using a single transducer and single hydrophone, which were used in conventional underwater communication systems, we added more hydrophones to improve the performance of the system. Then, we expanded our model by adding more users to increase our data rate.

In this thesis, we assumed that the channel is exactly known. We are in the process of designing a channel estimation algorithm using time reversal signaling. This approach helps us to estimate the underwater channel when we have slow time variations. The next step is to estimate the channel when we have more Doppler spread. Moreover, using this system for data transmission in millimeter wave would be the next step.

Appendices

Appendix A

Simulation Packages and Supplementary Programs

A.0.1 Channel Model

In order to run the Simulink simulation program, various channel matrices need to be generated. First, the Bellhop software provides us with the channel impulse responses of the received signal. Using this information,]*Model_run_MIMO_v2_loadbellhop.m* generates the time and frequency domain versions of the channel matrices.

The following program is an example of generating the channel matrices for one user and 5 hydrophones.

```
profile on
% MIMO, basic dynamic channel model, fixed analog
%tap delays, baseband
% no noise
% MIMO version, see far-field channel model notes
% this script set up paramaters, runs the SetState function for
% the modelto get the initial state
% then gets channel for a number of sample blocks
%
% author: Dmitry Trukhachev
% May 22, 2017
% May 23, 2017

% -- system parameters ------------------------------------------

% clear all;
% load 1km/example_2000Hz40m.mat;
rng('default');
```

```
% Bandwidth in Hz
SysPara.B = 320;
% Sample time (OFDM symbol time will be N times larger ...)
SysPara.Ts = 1/(SysPara.B);
% carrier frequency
SysPara.fc = 2048;

ascal = 1;

% oversampling factor in time domain
SysPara.fostime = 1;
% oversampling factor in delay domain
SysPara.fostau = 1;

% Filter type
SysPara.Filttype = 'RC';
% filter rolloff
SysPara.beta = 0.25;
% Total consumed bandwidth
SysPara.Btotal = SysPara.B *(1+SysPara.beta);
% window size of quantized filter impulse response coefficients

% analog path delays given IN SECONDS
[SysPara.taua1,index] = sort(arr_info.delay(1:arr_info.Narr));
%
%% normalize them per sample time, considering oversampling factor
SysPara.taua1 = SysPara.taua1 / (SysPara.Ts/SysPara.fostau);
SysPara.taua = SysPara.taua1 - SysPara.taua1(1);
% average path powers, not necessarily normalized
SysPara.h = arr_info.A(index);
% a : Shape parameter of the (stretched exponential)
%Doppler spectra (alpha)
```

```
SysPara.a = arr_info.NumTopBnc(index) * ascal;
% a : Shape parameter of the (stretched exponential)
%Doppler spectra (alpha)
%SysPara.CorrFlag =
%[0 0 1 2 0 0 5 6 0 0 9 10 0 0 13 14 0 0 17 18 0 0 21 22];
% number of paths
SysPara.Lp = length(SysPara.taua);

% average path powers, not necessarily normalized
SysPara.Pow = abs(SysPara.h).^2;
% number of paths
SysPara.Lp = length(SysPara.taua);

% departure angles for each analog path, given in radians
SysPara.Txangle = arr_info.SrcAngle(index)*pi/180;
% arrival angles for each analog path, given in radians
SysPara.Rxangle = arr_info.RcvrAngle(index)*pi/180;
% angles extracted from the phases of the analog channel taps
SysPara.hangles(1,1,:) = angle(SysPara.h);

% -- MIMO parameters ------------------------------------------
SysPara.Nt = 1;
SysPara.Nr = 5;

% assume low spacing at the Tx side and full correlation
SysPara.Txspacing = 0;
% assume low spacing at the Rx side
SysPara.Rxspacing = 0.32;

% compute delays and phases for all paths and Tx / rx pairs
[SysPara] = ChanMod_MIMO_DelaysPhases_v1(SysPara);
```

```
% flag : normalize output average! powers to
%sum up to 1 (yes 1, no 0)
SysPara.Pownorm = 'yes';

if (strcmp(SysPara.Pownorm, 'yes'))
SysPara.Pow = SysPara.Pow/sum(SysPara.Pow);
end

% Sum of sinusoids para
SysPara.M = 200;
% a : Shape parameter of the (stretched exponential)
%Doppler spectra (alpha)
SysPara.a = ones(1,SysPara.Lp) * .1;

% just for testing set the delay differences
%of the paths randomly and phases too

% -- simulation parameters ------------------------------------

N = 1024;

% total number of samples to generate
% this number includes oversampling in time domain
SimPara.NumSamp = N; % even

% set the longest tap (cutoff) based on analog path delays
% the taps are every 1/(SysPara.Ts/SysPara.fostau) seconds,
%i.e. every over sample in the delay domain
SimPara.Lmax = N;
%SysPara.phi = rand(SysPara.Nt,SysPara.Nr);

% do we normalize the power of each fading path per OFDM symbol?
```

```
SimPara.fadnorm = 'yes';

%--- testing the model ------------------------------------

% set the initial state
[State] = ChanMod_MIMO_SetState_v3(SysPara,SimPara);
%tic
% get the channel
% we just need one OFDM symbol
H = zeros(SysPara.Nt,SysPara.Nr,SimPara.Lmax,SimPara.NumSamp);
[State,H] = ChanMod_MIMO_GetChan_v1(SimPara,State,H);

% translate into frequency domain
H1 = squeeze(H(1,1,:,:));
% circular shifts ------------------------------------------
% first flip the rows of H1, the elements were going from left
%to right now they are from right to left
% transposition is used to exchange time vs delay dimensions
Hf1 = flip(H1',2);

% now we shift row i by i to the right ( i = 1, ..., N)
for i = 1:N
Hf(i,:) = circshift(Hf1(i,:),[0 i]);
end

grid = 0:N-1;
F = 1/sqrt(N) * exp( - 2* pi* 1i * (grid' * grid)/N);

Hf = F * Hf * F';

Model_MIMO_visual_v1(SysPara,H,N);
```

```
for j = 1:SysPara.Nr

H1 = squeeze(H(1,j,:,:));
% circular shifts ------------------------------------------
% first flip the rows of H1, the elements were going from
%left to right now they are from right to left
% transposition is used to exchange time vs delay dimensions
Hf1 = flip(H1',2);

% now we shift row i by i to the right ( i = 1, ..., N)
for i = 1:N
Hf(i,:) = circshift(Hf1(i,:),[0 i]);
end

Hf1 = F * Hf * F';
HF(1,j,:,:) = Hf1;
%Model_MIMO_visual_v1(SysPara,H,N);
end

HxFmat11(:,:) = HF(1,1,:,:);
HxFmat12(:,:) = HF(1,2,:,:);
HxFmat13(:,:) = HF(1,3,:,:);
HxFmat14(:,:) = HF(1,4,:,:);
HxFmat15(:,:) = HF(1,5,:,:);
RFmat11 = HxFmat11'*HxFmat11;
RFmat12 = HxFmat12'*HxFmat12;
RFmat13 = HxFmat13'*HxFmat13;
RFmat14 = HxFmat14'*HxFmat14;
RFmat15 = HxFmat15'*HxFmat15;

%The aggregation of R-matrices and off-diagonal elements.
```

```
RFmat1 = RFmat11+RFmat12+RFmat13+RFmat14+RFmat15;
RFoff1 = RFmat1 - diag(diag(RFmat1));

%
HxFmat21(:,:) = HF(1,1,:,:);
HxFmat22(:,:) = HF(1,2,:,:);
HxFmat23(:,:) = HF(1,3,:,:);
HxFmat24(:,:) = HF(1,4,:,:);
HxFmat25(:,:) = HF(1,5,:,:);
RFmat21 = HxFmat21'*HxFmat21;
RFmat22 = HxFmat22'*HxFmat22;
RFmat23 = HxFmat23'*HxFmat23;
RFmat24 = HxFmat24'*HxFmat24;
RFmat25 = HxFmat25'*HxFmat25;

%The aggregation of R-matrices and off-diagonal elements.
RFmat2 = RFmat21+RFmat22+RFmat23+RFmat24+RFmat25;
RFoff2 = RFmat2 - diag(diag(RFmat2));

%The matrices of interference from the other user
Sec_User_Int_30m1 = HxFmat11'*HxFmat12 + HxFmat12'*HxFmat22 +
 HxFmat13'*HxFmat23...
+HxFmat14'*HxFmat24 + HxFmat15'*HxFmat25;
Sec_User_Int_30m2 = HxFmat21'*HxFmat11 + HxFmat22'*HxFmat12 +
 HxFmat23'*HxFmat13...
+HxFmat24'*HxFmat14 + HxFmat25'*HxFmat15;
```

A.0.2 Repeat Accumulate Code

The following program also generates the parity check and generator matrices based on the theory in section 3.2. In order to implement the blocks in Figure **??**, we define three matrices. Matrix *Grep* for repetition code, *Gpi_int_comb* for interleaver and *Gacc* for accumulator blocks.

```
%Code settings
n=1024;
dv=6;
dc=6;
r=dc-2;
\textbf{code_rate=1/(1+dv/dc);

disp('Generator matrix and parity check matrix creation tool')
disp('Code settings:')
msg=['lenght of the information part: ', num2str(n)];
disp(msg)
msg=['repetition rate (d_v): ', num2str(dv)];
disp(msg)
msg=['check node degree (d_c): ', num2str(dc)];
disp(msg)
msg=['code rate: ', num2str(code_rate)];
disp(msg)
%Generator matrix
disp('Generator matrix')


%Repetition matrix
disp('creating repetition matrix (G_rep)')
Grep_init=eye(n);
Grep=zeros(n);
for i=1:1:n
for k=1:dv
```

```
Grep((i-1)*dv+k,:)=Grep_init(i,:);
end
end

%Interleaver matrix
disp('creating interleaver matrix (G_pi)')
Gpi=eye(n*dv);
interleave_vec=randintrlv(1:n*dv,randi(7815,1,1));
%interleave row indizes (random seed: 7815)
Gpi_int=Gpi(interleave_vec,:);
Gpi_int_comb=zeros(floor(n*dv/dc),n*dv);
for i=1:1:floor(n*dv/dc)
k=1;
while k<=dc && k<=length(Gpi_int(:,1))
Gpi_int_comb(i,:)=Gpi_int_comb(i,:)+Gpi_int(k,:);
Gpi_int(k,:)=[];
k=k+1;
end
end
%Accumulate matrix
disp('creating accumulator matrix (G_acc)')
Gacc=zeros(floor(n*dv/dc));
for i=1:1:floor(n*dv/dc)
for k=1:i
Gacc(i,k)=1;
end
end

disp('calculate final generator matrix')
generator_matrix=[eye(n) mod(Gacc*Gpi_int_comb*Grep,2)'];
```

```
%parity check matrix
disp('Parity check matrix')


%H1 matrix
disp('calculate H1 matrix')
H1=mod(Gpi_int_comb*Grep,2);

%H2 matrix
disp('calculate H2 matrix')
H2=zeros(floor(n*dv/dc));
for i=1:1:floor(n*dv/dc)
if i<floor(n*dv/dc)
for k=1:2
H2(i+k-1,i)=1;
end
else
H2(i,i)=1;
end
end

disp('calculate parity check matrix')
parity_check_matrix=[H1 H2];
disp('calculate sparse parity check matrix')
parity_check_matrix_s=sparse(parity_check_matrix);
[N_bit,N_coded_bit] = size(generator_matrix);
```

Bibliography

[1] C. Schlegel, *Waveform Communications*, ECED 3511 Lecture Notes, Dalhousie University, available at `www.umdcc.ca`.

[2] Christian Schlegel and Lance Perez, *Trellis and Turbo Codiing: Iterative and Graph-Based Error Control Coding*, IEEE/Wiley, 2015.

[3] C. Schlegel, *Research Day Summary: Iterative Receiver Concept*, Report, January 2017.

[4] C. Schlegel and M. Burnashev, *The interplay between error control coding and iterative signal cancelation*, IEEE Trans. Signal Proc., Vol. 65, No. 11, pp. 3020 3031, 2017.

[5] C. Schlegel et. al. *UMDCC Annual Report*, December 2016.

[6] C. Schlegel and M. Burnashev, "The interplay between error control coding and iterative signal cancelation," *IEEE Trans. Signal Proc.*, Vol. 65, No. 11, pp. 3020–3031, 2017.

[7] D. Trukhachev *UMDCC Report*, April 2017.